In situ structural studies and gas phase visualization of model catalysts at work

Blomberg, Sara

2017

In situ Structural Studies and Gas Phase Visualization of Model Catalysts at Work

Sara Blomberg

LUND UNIVERSITY

DOCTORAL DISSERTATION
by due permission of the Faculty of Science, Lund University, Sweden.
To be defended in Rydberg Lecture Hall. June 9, 2017 at 09.15

Faculty opponent
Prof. Dr. Peter Varga
Technische Universität Wien
Austria

Organization	Document name
LUND UNIVERSITY Synchrotron Radiation Research Department of Physics Box 118 SE-221 00 Lund Sweden	DOCTORAL DISSERTATION Date of issue 2017-06-09
Author(s) Sara Blomberg	Sponsoring organization

Title and subtitle

In situ Structural Studies and Gas Phase Visualization of Model Catalysts at Work

Abstract

This thesis reports on *in situ* structural studies relevant to a catalytic surface during CO oxidation. The materials that have been studied are palladium, rhodium and an alloy of palladium and silver, with applications in emission cleaning by catalytic converters in vehicles. The studies are performed *in situ* allowing for observation of the gas-surface interaction, which is essential when active catalysts are studied. Due to the vital role of the gas interaction for the surface structure, the gas phase in the vicinity of the catalytically active surface has also been studied in detail with spatial resolution using Planar Laser Induced Fluorescence, PLIF.

In this thesis, the CO oxidation reaction has been investigated by a step-by-step approach where the oxidation and reduction of the surfaces have first been studied separately. The systematic *in situ* oxidation studies at high pressure (up to 1 mbar) of the Pd, Rh and $Pd_{75}Ag_{25}$ provide information about oxide growth and the chemical composition of oxide structures that may be present during CO oxidation. To achieve a better understanding of the CO oxidation reaction, the gas distribution over the surface has been studied. The results show that the pressure, gas flow and the reaction itself determine the gas phase interacting with the surface, which influences the surface structure. At high gas flow and pressure, a boundary layer is formed in the mass transfer limited regime of CO oxidation, in which the gas composition is completely different from the gas composition measured by the mass spectrometer at the outlet of the reactor. If the conditions are oxygen rich, the CO concentration close to the surface, in this regime, is low. Nevertheless, a metallic Pd and Rh surface covered with chemisorbed oxygen is detected in a 1:1 ratio of CO and O_2 at total pressures up to 1 mbar. Only in more oxygen rich conditions (4:1 of O_2:CO), a surface oxide may be detected.

Key words

CO oxidation, model catalyst, PLIF, APXPS, Pd, Rh, PdAg

Classification system and/or index terms (if any)

Supplementary bibliographical information	Language English
ISSN and key title	ISBN 978-91-7753-301-6 (Print) 978-91-7753-302-3 (Pdf)
Recipient´s notes	Number of pages / Price Security classification

In situ Structural Studies and Gas Phase Visualization of Model Catalysts at Work

Sara Blomberg
Division of Synchrotron Radiation Research

LUND UNIVERSITY

Faculty of Science
Department of Physics

ISBN 978-91-7753-301-6 (Print)
978-91-7753-302-3 (Pdf)

Printed in Sweden by Media-Tryck, Lund University
Lund 2017

"to awaken affinities, which are asleep at a particular temperature,
by their mere presence and not by their own affinity"
Jöns Jacob Berzelius, 1835

Abstract

This thesis reports on *in situ* structural studies relevant to a catalytic surface during CO oxidation. The materials that have been studied are palladium, rhodium and an alloy of palladium and silver, with applications in emission cleaning by catalytic converters in vehicles. The studies are performed *in situ* allowing for observation of the gas-surface interaction, which is essential when active catalysts are studied. Due to the vital role of the gas interaction for the surface structure, the gas phase in the vicinity of the catalytically active surface has also been studied in detail with spatial resolution using Planar Laser Induced Fluorescence, PLIF.

In this thesis, the CO oxidation reaction has been investigated by a step-by-step approach where the oxidation and reduction of the surfaces have first been studied separately. The systematic *in situ* oxidation studies at high pressure (up to 1 mbar) of the Pd, Rh and $Pd_{75}Ag_{25}$ provide information about oxide growth and the chemical composition of oxide structures that may be present during CO oxidation. To achieve a better understanding of the CO oxidation reaction, the gas distribution over the surface has been studied. The results show that the pressure, gas flow and the reaction itself determine the gas phase interacting with the surface, which influences the surface structure. At high gas flow and pressure, a boundary layer is formed in the mass transfer limited regime of CO oxidation, in which the gas composition is completely different from the gas composition measured by the mass spectrometer at the outlet of the reactor. If the conditions are oxygen rich, the CO concentration close to the surface, in this regime, is low. Nevertheless, a metallic Pd and Rh surface covered with chemisorbed oxygen is detected in a 1:1 ratio of CO and O_2 at total pressures up to 1 mbar. Only in more oxygen rich conditions (4:1 of O_2:CO), a surface oxide may be detected.

Populärvetenskaplig sammanfattning

Katalys används vid 90% av all produktion av kemikalier och är därtill anledningen till att utsläppen av kolmonoxid och kväveoxider drastiskt har minskat i transportsektorn. En katalysator fungerar som en ”genväg” för en kemisk process, genom växelverkan mellan gasmolekyler och ytan av en katalysator kan den kemiska reaktionen ske till en lägre energikostnad. Detta innebär att sannolikheten att den kemiska reaktionen ska ske under vissa specifika förhållanden är större med än utan en katalysator. Katalysatorn själv förbrukas inte under reaktionen, utan kan fungera under lång tid. För att effektivisera en katalysator eller utveckla helt nya katalysatorer, krävs en mer grundläggande kunskap om växelverkan mellan det katalytiska materialet och gas molekylerna. Detta åstadkoms genom att studera modellsystem av mycket komplexa industriella katalysatorer och katalytiska processer. Dessa experiment har under många år utförts i så kallat Ultra-Högt Vakuum (UHV) vilket gör det möjligt att studera katalys på en atomär nivå. Professor G. Ertl belönades med nobelpriset i kemi år 2007 för sina studier av modellsystem för katalytiska processer.

Eftersom de flesta tillämpningar av katalys sker vid atmosfärstryck och högre tryck är det relevant att utföra experiment vid mer katalytiskt realistiska förhållanden. I denna avhandling har framförallt högtrycksfotoelektronspektroskopi använts för att studera kemiska processer, relevanta för CO-oxidering, på ytan av modellkatalysatorer. CO-oxidering är en av de enklare kemiska processer som sker i en bilkatalysator men hur processen går till i detalj, är fortfarande oklart. Vi har därför använt de enklaste modellsystem i form av enkristaller för att få fram mer grundläggande information om processen. Även nanopartiklar har studerats vilket är ett steg mot hur industriella katalysatorer faktiskt ser ut.

Användningen av högtrycksfotoelektronspektroskopi gör det möjligt att följa kemiska ytprocesser ”live”. Vi har därför kunnat konstatera att komplexa syrestrukturer är mycket effektiva i CO-oxideringsprocessen, vilket är relevant för industriella katalytiska system. Vi har även studerat en legering som ser ut att vara

en mycket lovande och effektiv katalysator för CO-oxidering men som är billigare att framställa.

Eftersom fler och fler ytfysikstudier utförs vid högre tryck är det även intressant att förstå hur gasblandningen förändras nära den aktiva katalysatorns yta. Vi har därför vidareutvecklat en laserbaserad teknik kallad laser inducerad flourescensens med tillhörande reaktorer, för att studera gasfasen under katalytiska förhållanden. Med hjälp av denna laserdiagnostiska teknik kan man följa resultatet av den katalytiska processen även i gasfasen och på så sätt länka samman gassammansättningen som växelverkar med ytan och ytans struktur. I Figur 1 illustreras hur våra mätnignar av ytstrukturen och gasmolekylerna kan ge en mer komplett bild av hur den kemiska reaktionen sker på en katalytiskt aktiv yta, något som vi tror i framtiden kan leda till nya, bättre, billigare och mer energisnåla katalysatorer.

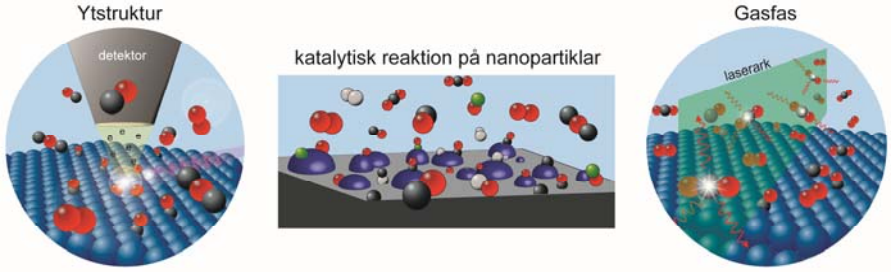

Figur 1. Den mycket komplicerade industriella katalytiska rekationen använder nanopartiklar som katalysator och måste förenklas för att kunna studera specifika egenskaper hos ytan eller hos gas molekylerna. Vi tittar på välordnade modellkatalysatorer för att få information om ytstrukturer på katalysatorn. För att även förstå hur gas molekylerna påverkar katalysatorn använder vi en laser för att undersöka detta.

Preface and List of publications

This doctoral thesis presents my contribution to the field of catalysis and CO oxidation over transition metals. The *in situ* studies of catalysts at work provide information about its surface as well as the gas phase. The experiments are performed at pressures and temperatures approaching more realistic conditions for an operating industrial catalyst motivated by a strive to understand the reaction that occurs on an industrial catalyst on the atomic scale. The experiments concerning surface structures are performed at large scale synchrotron radiation facilities (MAX IV-Sweden, Bessy-Germany, and ALS-USA) and the gas phase experiments at Lund Laser Centre.
Part of the work has previously been presented in my licentiate thesis "Planar Laser Induced Fluorescence, and High Pressure X-ray Photoelectron Spectroscopy applied to CO oxidation over model catalysts."

The thesis is based on the following papers, which are referred to in the text by their Roman numerals.

I. **Oxidation and reduction of Pd(100) and aerosol-deposited Pd nanoparticles**
R. Westerström, M. E. Messing, S. Blomberg, A. Hellman, H. Grönbeck, J. Gustafson, N. M. Martin, O. Balmes, R. van Rijn, J. N. Andersen, K. Deppert, H. Bluhm, Z. Liu, M. E. Grass, M. Hävecker and E. Lundgren
Phys. Rev. B. **83** (2011) 115440
I took part in the Photoelectron Spectroscopy measurements and the discussion about the results and conclusions for the manuscript.

II. **A high pressure X-ray photoelectron spectroscopy study of oxidation and reduction of Rh(100) and Rh nanoparticles**
S. Blomberg, R. Westerström, N. M. Martin, E. Lundgren, J. N. Andersen, M. E. Messing and J. Gustafson,
Surf. Sci. **628** (2014) 153–158
I planned and took part in the Photoelectron Spectroscopy measurements. I was responsible for analyzing the spectroscopy data and wrote the manuscript.

III. **Surface composition of clean and oxidized $Pd_{75}Ag_{25}$(100) from photoelectron spectroscopy and density functional theory calculations**
L. E. Walle, H. Grönbeck, V. R. Fernandes, S. Blomberg, M. H. Farstad, K. Schulte, J. Gustafson, J. N. Andersen, E. Lundgren and A. Borg,
Surf. Sci. **606** (2012) 1777-1782
I took part in the Photoelectron Spectroscopy measurements and the discussion about the manuscript.

IV. **Reduction behavior of oxidized Pd(100) and $Pd_{75}Ag_{25}$(100) surfaces using CO**
V. R. Fernandes, J. Gustafson, I -H. Svenum, M. H. Farstad, L. E. Walle, S. Blomberg, E. Lundgren and A. Borg,
Surf. Sci. **621** (2014) 31–39
I took part in the Photoelectron Spectroscopy measurements.

V. **Generation and oxidation of aerosol deposited PdAg nanoparticles**,
S. Blomberg, J. Gustafson, N. M. Martin, M. E. Messing, K. Deppert, Z. Liu, R. Chang, V.R. Fernandes, A. Borg, H. Grönbeck and E. Lundgren,
Surf. Sci. **616** (2013) 186–191
I planned and took part in the Photoelectron Spectroscopy measurements. I was responsible for analyzing the spectroscopy data, and I wrote the manuscript.

VI **_In situ_ X-ray Photoelectron Spectroscopy of Model catalysts: At the Edge of the Gap**
S. Blomberg, M. J. Hoffmann, J. Gustafson, N. M. Martin, V. R. Fernandes, A. Borg, Z. Liu, R. Chang, S. Matera, K. Reuter and E. Lundgren.
Phys. Rev. Lett. **110** (2013) 117601
I took part in the Photoelectron Spectroscopy measurements and was responsible for analysing the spectroscopy data. I wrote part of the manuscript.

VII. **A high pressure X-ray photoelectron spectroscopy study of CO oxidation over Rh(100)**
J. Gustafson, S. Blomberg, N. M. Martin, V. Fernandes, A. Borg, Z. Liu, R. Chang and E. Lundgren,
J. Phys.: Condens. Matter **26** (2014) 055003
I planned and took part in the Photoelectron Spectroscopy measurements.

VIII. **An _in situ_ set up for the detection of CO_2 from catalytic CO oxidation by using planar laser induced fluorescence**
J. Zetterberg, S. Blomberg, J. Gustafson, Z. W. Sun, Z. S. Li, E. Lundgren and M. Aldén,
Rev. Sci. Instrum. **83** (2012) 053104
I planned and took part in the Laser-Induced Fluorescence measurements. I took part in the analyzing process of the data and writing of the manuscript.

IX. **Spatially and temporally resolved gas distributions around heterogeneous catalysts using infrared planar laser-induced fluorescence**
J. Zetterberg, S. Blomberg, J. Gustafson, J. Evertsson, J. Zhou, E. C. Adams, P. A. Carlsson, M. Aldén, E. Lundgren,
Nat Commun **6** (2015) 7076
I planned and took part in the Laser-Induced Fluorescence measurements. I took part in the analyzing process and writing of the manuscript.

X **Real-Time Gas-Phase Imaging over a Pd(110) Catalyst during CO Oxidation by Means of Planar Laser-Induced Fluorescence**
S. Blomberg, C. Brackmann, J. Gustafson, M. Aldén, E. Lundgren and J. Zetterberg,
ACS Catal. 5 (2015) 2028–2034
I planned and took part in the Laser-Induced Fluorescence measurements. I took part in the analyzing process and was responsible for the interpretation of the results as well as writing of the manuscript.

XI. **Comparison of AP-XPS and PLIF Measurements During CO Oxidation Over Pd Single Crystals**
S. Blomberg, J. Zetterberg, J. Gustafson, J. Zhou, C. Brackmann and E. Lundgren,
Top Catal 59 (2016) 478–486
I planned and took part in the Photoelectron Spectroscopy as well as the Laser-Induced Fluorescence measurements. I was responsible for analyzing the Photoelectron spectroscopy data and interpret the Laser-Induced Fluorescence results. I wrote the manuscript.

XII. **Evidence for the Active Phase of Heterogeneous Catalysts through In Situ Reaction Product Imaging and Multiscale Modeling**
S. Matera, S. Blomberg, M. J. Hoffmann, J. Zetterberg, J. Gustafson, E. Lundgren and K. Reuter,
ACS Catal. 5 (2015) 4514-4518
I planned and took part in the Laser-Induced Fluorescence measurements.

XIII. **2D and 3D imaging of the gas phase close to an operating model catalyst by planar laser induced fluorescence**
S. Blomberg, J. Zhou, J. Gustafson, J. Zetterberg and E. Lundgren,
J. Phys.: Condens. Matter **28** (2016) 453002
I planned and took part in the Laser-Induced Fluorescence measurements. I took part in the analyzing process and was responsible for the interpretation of the results as well as writing the manuscript.

XIV. **Strain Dependent Light-off Temperature in Catalysis Revealed by Planar Laser-Induced Fluorescence**
S. Blomberg, J. Zetterberg, J. Zhou, L. R. Merte, J. Gustafson, M. Shipilin, A. Trinchero, L. A. Miccio, A. Magaña, M. Ilyn, F. Schiller, J. E. Ortega, F. Bertram, H. Grönbeck and E. Lundgren
ACS Catal. 7 (2017) 110-114
I planned and took part in the Photoelectron Spectroscopy as well as the Laser-Induced Fluorescence measurements. I was responsible for analyzing the Photoelectron Spectroscopy data as well as the interpretation of the results from the Laser-Induced Fluorescence measurements. I wrote the paper.

XV. **Visualization of Gas Distribution in a Model AP-XPS Reactor by PLIF: CO Oxidation over a Pd(100) Catalyst**
J. Zhou, S. Blomberg, J. Gustafson, E. Lundgren and J. Zetterberg, Catalysts 7 (2017) 29
I planned and took part in the Laser-Induced Fluorescence measurements. I took part in the evaluation of the data and the discussion about the manuscript.

XVI. **Combining synchrotron light with laser technology in catalysis research**
S. Blomberg, J. Zetterberg, J. Gustafson, J. Zhou, M. Shipilin, S. Pfaff, U. Hejral, P.A. Carlsson, O. Gutowski, U. Ruett and E Lundgren
In manuscript
I planned and took part in the measurements. I took part in the interpretation of the results as well as being responsible for writing the manuscript.

Related work

XVII. **Generation of Pd model catalyst nanoparticles by spark discharge**
M. E. Messing, R. Westerström, B. O. Meuller, S. Blomberg, J. Gustafson, J. N. Andersen, E. Lundgren, R. van Rijn, O. Balmes, H. Bluhm and K. Deppert,
J. Phys. Chem. C **114** (2010) 9257

XVIII. **Carbonate formation on p(4 × 4)-O/Ag(111)**
J. Knudsen, N. M. Martin, E. Grånäs, S. Blomberg, J. Gustafson, J. N. Andersen, E. Lundgren, S. Klacar, A. Hellman and H. Grönbeck, Phys. Rev. B **84** (2011)115430.

XIX. **High resolution core level spectroscopy study of the ultrathin aluminum oxide on NiAl(110)**
N. M. Martin, J. Knudsen, S. Blomberg, J. Gustafson, J. N. Andersen, E. Lundgren, H. Härelind Ingelsten, P. -A. Carlsson, M. Skoglundh, A. Stierle and G. Kresse,
Phys. Rev. B. **83** (2011) 125417.

XX. **Oxygen interaction with the Pd(112) surface: from chemisorption to bulk oxide formation**
A. Vlad, A. Stierle, R. Westerström, S. Blomberg, A. Mikkelsen, and E. Lundgren,
Phys. Rev. B **86** (2012) 035407

XXI. **Structure of the Rh_2O_3(0001) surface**
S. Blomberg, E. Lundgren, R. Westerström, E. Erdogan, N. M. Martin, A. Mikkelsen, J. N. Andersen, F. Mittendorfer and J. Gustafson,
Surf. Sci. **606** (2012) 1416

XXII. **Bulk characterization and surface properties of In_2O_3(001) single crystals**
D. Hagleitner, P. Jacobson, S. Blomberg, K. Schulte, E. Lundgren, M. Kubicek, J. Fleig, F. Kubel, L. A. Boatner, M. Schmid, U. Diebold, Phys. Rev. B. **85** (2012) 115441

XXIII. **Reversible formation of a PdC_x phase in Pd nanoparticles upon CO and O_2 exposure**
O. Balmes, A. Resta, D. Wermeille, R. Felici, M. E. Messing, K. Deppert, Z. Liu, M. E. Grass, H. Bluhm, R. van Rijn, J. W. M. Frenken, R. Westerström, S. Blomberg, J. N. Andersen, J. Gustafson and E. Lundgren,
Chem. Phys. Phys. Chem. **14** (2012) 4796

XXIV. **Dissociative adsorption of hydrogen on PdO(101) studied by HRCLS and DFT**
N. M Martin, M. van den Bossche, H. Grönbeck, C. Hakanoglu, J. Gustafson, S. Blomberg, M. A. Arman, A. Antony, R. Rai, A. Asthagiri, J. F. Weaver and E. Lundgren,
J. Phys. Chem. C **117** (2013) 167

XXV. **Facile NOx interconversion over preoxidized Ag(111)**
S. Klacar, N. M. Martin, J. Gustafson, S. Blomberg, Z. Liu, S. Axnanda, R. Chang, E. Lundgren and H. Grönbeck,
Surf. Sci. **617** (2013) 167

XXVI. **High-coverage oxygen-induced surface structures on Ag(111)**
N. M. Martin, S. Klacar, H. Grönbeck, J. Knudsen, J. Schnadt, S. Blomberg, J. Gustafson and E. Lundgren,
J. Phys. Chem. C **118** (2014) 15324

XXVII. **H_2 reduction of surface oxides on Pd-based membrane model systems-The case of Pd(100) and $Pd_{75}Ag_{25}$(100)**
V. R. Fernandes, J. Gustafson, M. H. Farstad, L. E. Walle, S. Blomberg, E. Lundgren, H. J. Venvik and A. Borg,
Appl. Surf. Sci. **313** (2014) 794

XXVIII. **Intrinsic Ligand Effect Governing the Catalytic Activity of Pd Oxide Thin Films**
N. M. Martin, M. van den Bossche, A. Hellman, H. Grönbeck, C. Hakanoglu, J. Gustafson, S. Blomberg, N. Johansson, Z. Liu, S. Axnanda, J. F. Weaver and E. Lundgren,
ACS Catal. **4** (2014) 3330

XXIX. **Growth of Ultrathin Iron Oxide Films on Ag(100)**
L. R. Merte, M. Shipilin, S. Ataran, S. Blomberg, C. Zhang, A. Mikkelsen, J. Gustafson and E. Lundgren,
J. Phys. Chem. C 119 (2015) 4514

XXX. **Planar Laser Induced Fluorescence Applied to Catalysis**
J. Zetterberg, S. Blomberg, J. Zhou, J. Gustafson and E. Lundgren,
book chapter in "*Operando Research in Heterogeneous Catalysis*", edited by J. Frenken and I Groot,
Springer Series in Chemical Physics **114,** Switzerland, (2017) pp 131-148

Acknowledgements

During the time of writing of my thesis I have had a chance of looking back at the time I've spent at the division of synchrotron radiation research and realized that I've spent almost a third of my life together with you at Fysicum. Each paper contributing to this thesis has its own story, which has of course included blood sweat and tears but also new friends and colleagues, which I would like to take the opportunity to thank.

First of all, I would like to acknowledge my supervisor, *Prof. Edvin Lundgren*. The scientific result of almost ten years of collaboration, is presented in here, Edvin. I think 10 years and this thesis speak for itself - that I have had a great time and really enjoyed the time as a student! I appreciate that you encourage me to do my best in all situations and have supervised me in a professional way. The possibility of going to conferences and beamtime all over the world has been great fun but also inspiring. However, I also appreciate your goodwill and encouragement and your understanding of the difficulties of combining research and family.

I also would like to acknowledge my co-supervisor *Dr Johan Gustafson.* Your door is always open and our discussions about oxides, activity vs reactivity, basic physics concepts (I think I could continue to the end of this page) and much more, have been motivating and inspiring. I think the phrase "there are no stupid questions" would summaries our discussions quite well. You have taught me a lot, everything, from skiing to reciprocal space but you failed, however, to teach me "Så bistert kall…" but I hope I can get more opportunities in the future for more practicing.

We started more or less at the same time as PhD students at the division, and with the same supervisors, *Natalia*. Because of that we have had a lot of joined beamtimes, conferences and projects over the years you spent in Lund. You have been a great roomie and you are an easy going person, making traveling more fun. I think you enjoy shopping in San Francisco as much as I do, but I have to admit that I'm impressed with the way you packed you bags to be able to bring everything back to Sweden! *Elin*, we haven't done any scientific work together but we've shared the work of bringing the division together for different activities. For me that's contributing to an open atmosphere at the division, making long days in the lab a little bit easier. We were a bunch of PhD students that started within a year

from each other. However, *Olof,* you and I actually started the same day, but it wasn't until the last year that you became my roommate. Thanks for always keeping up a good spirit at the office and giving me good advice when I've needed it. Our Nashville and the Elvis trip is something to remember when Christmas is closing in. Talking about memorable moments with Santa Claus, this gives me the opportunity to thank *Patrik*. What would life be without strong opinions and gossip? It is great to have you around the coffee table, keeping me updated of what's going on at "Fejan" or in the news. I appreciate your help when it comes to complicated paperwork but also that you always prioritize the PhD students.
Chu Chu and *Sofie,* when you started as PhD students we were roommates, which had consequences for our everyday life. Soon, our office became the known as "the mom's office" and we could share our stories and experiences about our "treasures". Sharing the experience of combining research and family made it somehow a little easier. *Mikhail* and *Uta* thanks for being such a diffraction gurus helping out in the lab and in the evaluation of the data. *Lindsay*, thanks for fruitful discussions about the analysis of the data and for valuable comments in the writing process of the manuscripts. *Jonas*, I still remember when we were discussing your bachelor project at "Rydan" some years back. We spent quite some time in the laser lab together and you have contributed to get the PLIF measurements going. I hope you have continued with the scrapbooking skills I taught you for the logbook! *Johan K*, thanks for your invaluable comments about life whenever you are knocking at our office door. *Rasmus,* you helped me a lot during my first years as a bachelor and master student at the division. It is great to see you back in time for my defence, which I realize is almost exactly 7 years after you (only two days differ). I would also like to thank you *all* at Sljus for making the division to a great workplace. *Maria Messing*, you are the first author of my first paper as co-author. That was a milestone for me! You have also introduced me to the "nanoworld", by providing nanoparticle samples and by teaching me SEM in the cleanroom. I also would like to thank you for being such a good roomie at the conferences.

I have always felt welcome to the division of Combustion Physics and many friends are working there. I'm therefore glad that I finish my PhD studies with a strong connection to your division both personally but also through joint projects. I would like to thank *Marcus Aldén* for making our laser campaigns possible, it has been great fun but also very successful to extend my catalysis studies into your labs. I would also like to thank *Christian Brackmann* that has contributed with a lot of the PLIF images that has been shown in papers and at conferences. We were working hard, with a table fan and other very advanced methods, to keep the laser running, but " skam den som ger sig". I would like to acknowledge *Jianfeng*, you

have contributed a lot to this thesis. Not only by papers but also by providing me with images and plots whenever I've asked for them with nothing but a "No problem" and a smile. You're a hard working person with high ambitions, which is clear when looking at all improvement that has been made in the lab and in the data analysis. I would like to acknowledge the people at Maxlab or MAX IV. The open atmosphere and friendly staff is definitely something I will remember.

During we years at the division I have had the opportunity to travel a lot and by that I've made friends and colleagues all over the world. Starting in Sweden, I would like to thank all of you at KCK at Chalmers for great meetings and workshops. A special thanks to *Henrik Grönbeck* for the theoretical contribution to my papers but also for explaining your theoretical work in a way that an experimentalist can understand. *P.A (Per-Anders) Carlsson* I like your creativity and that you always come up with new ideas for experiments or setups. You have helped us in the lab by delivering catalysts samples and by that also making our research more applied. *Anne Borg, Mari Farstad, Lars Erik Walle, Vasco Fernandes* and *Marie Døvre* are all doing research in Trondheim but every now and then we meet up for beamtimes or at conferences. We have spent some time at 311 at Maxlab and long nightshift are always more inspiring working with a group of eager Norwegians. I have also worked with *Karsten Reuter, Sebastian Matera* and *Max Hoffmann* from Munich. I appreciate your enthusiasm of our operando studies and your simulated data are sometimes almost in too good agreement to believe it. *Hendrik Bluhm* introduced APXPS to me in 2009 and you did such a good job that I have continued working with XPS ever since. I appreciate that you took your time helping me with everything from technical questions about XPS to showing me the best lunch place in Berkeley. After 2009 I have been back in Berkeley and the ALS for many beamtimes but then at *Zhi Liu's* beamline. Thanks for always helping out whenever we needed it, making the best of our beamtime. I would like to thank the *staff at the ALS*. The next synchrotron I've spent some time on, is the ESRF where *Olivier* was working at that time. Thanks for having the patience to teach me how to acquire diffraction data and for planning the beamtime in such a good way that we had time to visit some nice restaurants in Grenoble. Next stop, is Leiden in the Netherlands where *Gertjan* is working. Thanks for you expertise in designing reactors and other components to our setup.

In Lund, I've also been a member of the Physics & Lasershow. We have had so much fun over the years. Going on tour is something special and the group became like a family. Thanks to all of you, *Malin*, *Stina*, *Ellinor*, *Violetta*, *Johan*, *Odd*, *Magnus*, *Martin* and *Elias*. In this section I also would like to acknowledge *PO* and

Tomas, for making the undergraduate studies inspiring and UDIF a place where you always feel welcome, with a great social atmosphere.

Malin, we have been friends almost since the first day I came to Lund. Thanks for supporting me whenever I needed it during the years. Having you close during the years as a PhD student has meant a lot to me.

I would also like to thank my family, my mom *Lisbeth*, my dad *Arne* and my two sisters *Linda* and *Maria*, for always supporting me, no matter what. Even though I decided to move to Lund, far away from you, I've always felt your unquestionable love. Your encouraging spirit has strengthened me and without you, I would not be where I am today!

I would also like to take the opportunity to thank *Pelle* and *Anette*. The last year has been intense and your support have been invaluable.

I've saved my warmest and most loving thanks for last. *Johan*, *Astrid* and *Hampus*, you are my biggest source of energy and inspiration. Thanks, *Johan*, for everything, making this dissertation possible. I admire you both as an inspiring and encouraging colleague and as a loving father to Astrid and Hampus.

Contents

Abstract vii

Populärvetenskaplig sammanfattning ix

Acknowledgements xix

Contents xxiii

1 Introduction 1

1.1 Catalysis and surface science 2
1.2 This work 4

2 Model catalysts 5

2.1.1 Single crystal surfaces 6
2.1.2 Vicinal surfaces 7
2.1.3 Cylindrically shaped crystal 9
2.1.4 Nanoparticles 10
2.1.5 Alloy Surfaces 11

3 Surface structures 13

3.1 Adsorbate induced structures 13
3.1.1 CO induced structures 14
3.1.2 Chemisorbed oxygen structures 14
3.1.3 Surface oxides 15

4 Heterogeneous catalysis 19

4.1 Reactivity of transition metals 19
4.2 CO oxidation 21
4.3 The change of the gas composition during the catalytic reaction 22

5 Experimental methods 25

5.1 X-ray Photoelectron Spectroscopy 25
5.1.1 Principle of operation 26
5.1.2 Spectrum Deconvolution 28

5.1.3 Ambient Pressure X-ray Photoelectron Spectroscopy under semi-realistic reaction conditions 30
5.2 Planar Laser Induced Fluorescence 33
5.2.1 Principle of operation 34
5.2.2 CO and CO_2 35
5.2.3 Experimental setups 38
5.3 Gas visualization in the MTL regime 41
5.4 Spatial resolution of the gas phase 41
5.5 Surface characterization methods 45
5.5.1 Scanning Tunneling Microscopy 46
5.5.2 Low Energy Electron Diffraction 47
5.5.3 Density Functional Theory 48
6 Conclusions and Outlook 49
References 53
Summary of papers 67
Oxidation and reduction of transition metals 67
Structural studies of a catalyst during CO oxidation 69
Gas phase visualization in the vicinity of a catalyst surface 70

1 Introduction

Catalysis is involved in the majority of all chemical processes and according to estimates, 90% of all industrially produced chemicals, such as fuel, plastics, pharmaceuticals, and fertilizers, are manufactured using catalysts[1]. The wide use of catalysts in the industry is due to the enhanced reaction rate or selectivity of the catalysed chemical process, resulting in many orders of magnitude higher production output, which is of great interest for society.

In 1835, Jöns Jakob Berzelius used the word *catalytic*[2] to described the chemical process of converting starch to sugar by acid, the decomposition of hydrogen peroxide by metals and the conversion of ethanol to acetic acid by Pt[3]. Since then, for almost 200 years the catalytic properties of materials have been investigated intensively. In 1909 Wilhelm Ostwald was awarded the Nobel Prize in chemistry for his work on catalysis. Ostwald had by then proposed a definition of the catalytic process that is still used today: "A catalyst is a substance that affects the rate of a chemical reaction without being part of its end products"[4]. Since then, the importance of catalytic reactions for society has reach unprecedented heights, and related research has resulted in several Nobel prizes, the latest rewarded to Gerhard Ertl in 2007[5]. In constrast to most catalysis studies, which is performed in a trial-and-error approch due to the complexity of the chemical processes, surface scientists study the reactions on model systems to gain fundamental understanding of the catalytic reaction at surfaces. An increased knowledge on an atomic level about reactions and the active phase of an operating catalyst could contribute to minimizing the catalysts production costs as well as keeping harmful emissions low, by increasing the efficiency and selectivity of the catalysts.

1.1 Catalysis and surface science

In heterogeneous catalysis, the catalyst and reactants are in different phases such as a solid catalyst reacting with molecules in the gas phase. The catalyst is used to accelerate a chemical reaction by providing an alternative pathway for the reaction. The pathway proceeds usually via adsorption of the reactants on the catalyst surface, which lowers the energy barriers in one of the reaction steps. The catalyzed reaction occurs therefore more likely as compared to the uncatalyzed case, see Figure 1:1. The adsorption of the reactants as well as desorption of the product on the catalyst surface are crucial steps in the catalytic process and is governed by the surface's geometric and electronic structure. Hence, to act as a good catalyst, the surface structure is essential. The aim of the surface science approach to catalysis is to contribute with fundamental knowledge about the surface properties, revealing why certain sites are catalytically active or inactive.

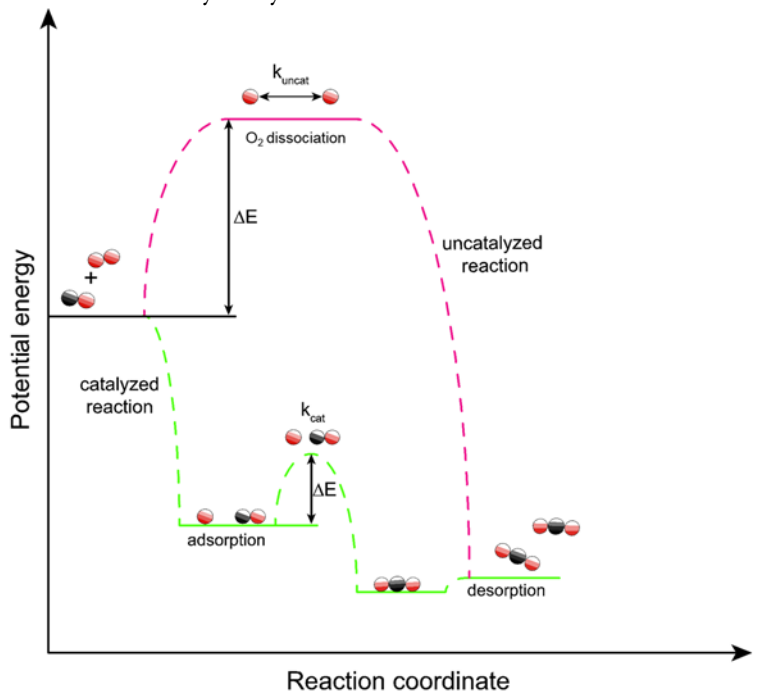

Figure 1:1 Schematic reaction diagram of CO oxidation with and without a catalyst. For the catalysed path, the activation energy ΔE is determined by the possibilities for O to react with CO via diffusion on the surface. For the uncatalyzed reaction, the O_2 dissociation is the energy needed for the reaction to proceed.

In an industrial reactor, the catalyst that consists of nanoparticles embedded in a porous oxide, is exposed to a harsh environment, including both high pressures and high temperatures. The low surface energy of the oxides as compared to the metal results in the nanoparticle formation on the surface. This keeps the surface to bulk ratio high, which is important since the catalytic reaction occurs on the surface. The catalytic chemical process is complex and in most cases not fully understood. Simplified model systems are therefore used for catalyst studies where the gas phase and the catalytically active surface often are investigated separately. To gain fundamental knowledge about the surface atoms involved in the chemical reaction, single crystals are often used. These crystals can be manufactured such that they expose a flat and well-defined surface, making it possible to study specific surface sites or surface structures and how they contribute to the catalytic activity. To study the interaction between the gas molecules and specific surface sites, surface science studies are often performed *ex situ* or during exposure to low pressures, typically ranging from 10^{-10} mbar to 10^{-6} mbar. When studies are performed *ex situ*, the surfaces are exposed to gasses with well-controlled partial pressures and temperatures during specific times. The gasses are then pumped away, and the sample is often cooled down to room temperature or even lower before the measurement is performed.

The simplified model catalysts differs significantly from the very complex oxide supported nanoparticles in industrial catalysts, which is referred to as the materials gap. The studies of the simplified models are as mentioned above, often performed at low pressures in contrast to the operating conditions for industrial catalysts, which is usually at atmospheric pressures or above. This is called the pressure gap.

One of the challenges in surface science is to link the results achieved from these simplified models studies performed at low pressures, to the industrial catalysts. One approach to bridge the materials as well as the pressure gap is to study well-defined, in size and shape, nanoparticles *in situ* or *operando* under more realistic conditions. Increasing the pressure is challenging from a technical point of view due to the low pressure required when electron-based techniques are used. These techniques utilizes the short mean-free-path of the electrons, making it possible to probe the first atomic layers of a material and therefore suitable for surface science studies. During the last decades, developments of these techniques have made it possible to operate electron-based techniques at more realistic pressures.

CO oxidation is an important reaction in the automotive catalyst to transform toxic CO to the less harmful CO_2. The two diatomic reactants of CO and O_2 makes the reaction comparatively simple and therefore also appropriate for surface science studies where fundamental information on an atomic level is desirable [6]. The reaction has therefore been studied in great detail for several decades[7, 8]. Despite this, the reaction mechanism is still not fully agreed upon, and the reaction pathway, via the catalyst surface, has been under debate for many years.

1.2 This work

The results presented in this work are achieved from *in situ* experiments, where the oxidation and reduction process of the surface is followed while it takes place. A gradually more oxidized or reduced surface is detected over time, and by that, a more complete picture of the oxide growth or reduction, can be obtained. To be able to determine the active phase of the catalyst, the surface structure should be probed while the reactants in the gas phase interact with the surface. It might be that the most active surface structure is only present when the reactants in the gas phase are surrounding the surface. For catalysis studies, *operando* measurements are therefore performed. The surface structure and the gas phase are investigated during the catalytic reaction by using Ambient Pressure X-ray Photoelectron Spectroscopy (APXPS). Due to its crucial impact on the surface structure and relevance for *operando* studies, the gas phase and in particular the gas distribution in the vicinity of the catalyst surface during the reaction has been studied in 2D by the means of Planar Laser-Induced Fluorescence (PLIF).

2 Model catalysts

The transition metals such as Pd, Pt, and Rh are often used as the active material in oxidation catalysts.[7, 9] These metals are rare in nature and therefore also very expensive. To minimize the manufacturing cost, in parallel with producing a very efficient catalyst, a maximized surface area of the metal is preferred. This can be achieved by producing metal nanoparticles. The atoms located at edges and corners of the particle have less neighboring atoms as compared to the atoms on the flat facets which in turn have less neighboring atoms than the atoms in the bulk, see Figure 2:1. The reduced coordination number have shown to have consequences for the reactivity that play an important role in catalytic reactions[10-15].

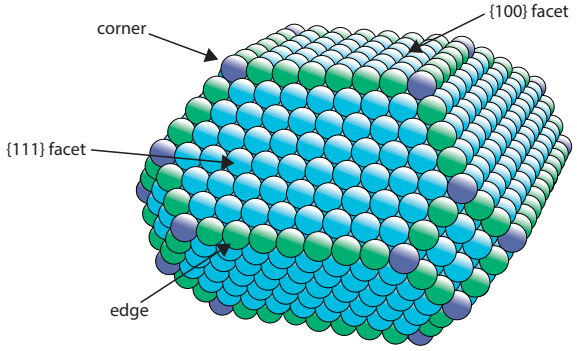

Figure 2:1 Model of a particle with (100) and (111) facets dominating the surface. The edges and corners consists of undercoordinated atoms and are therefore more reactive as compared to the atoms with more neighboring atoms.

The material complexity of industrial catalysts makes surface studies challenging, and simplified models are therefore used. One way of simplifying the system is to use a single crystal. The complexity of the model system can be increased by using vicinal surfaces or controlled deposition of well-characterized nanoparticles. This allows for a step by step approach towards fundamental understanding of an industrial catalyst under operating conditions[16 17].

2.1.1 Single crystal surfaces

In a crystal, the atoms are arranged in specific building blocks that repeat periodically in all three dimensions. One building block describes the smallest geometry of atoms from which the entire crystal can be constructed and is called the unit cell. Metal crystal structures, studied in this thesis, can be described by a cubic unit cell constructed by a coordinate system with three axes $\mathbf{a}_1$, $\mathbf{a}_2$ and $\mathbf{a}_3$ shown in Figure 2:2. In a simple cubic (sc) unit cell, an atom is located in each corner of a cube and by adding an atom in the center of the cube, the structure is called body-centered cubic (bcc). An atom can instead be added in the center of each side of the unit cell, it is referred to as a face-centered cubic structure (fcc). If the cubic unit cell is aligned with the same orientation in the entire sample, it is called single crystal. The cubic unit cell describes the bulk crystal structure, but the lack of neighboring atoms in one direction for the surface atoms gives the surface atoms other properties than the bulk atoms. A two-dimensional unit cell is therefore used to describe the structure of the surface atoms explicitly. The surface atoms construct a crystal plane, denoted by the shortest vector with integer coordinates normal to a plane or surface. This vector is described by the Miller indices *(hkl)*, which indicates where the plane intercepts with cubic unit cell axis $\mathbf{a}_1$, $\mathbf{a}_2$ and $\mathbf{a}_3$. Based on the known atomic arrangement in the cubic unit cell, the surface structure can be determined from vectors based on the Miller indices[18, 19]. To generate an atomically flat surface the crystal is cut in one of the cubic basal planes (100), (110) or (111), shown in Figure 2:2 and the surface is then referred to as a low-index surface. The low-index surfaces are the most well-defined surfaces and often used in surface science for fundamental studies. The well-defined surface allows for highly controlled experiments where the properties of single atoms in the surface can be deduced.

In this thesis, low index (100) surfaces of Pd, Rh as well as the alloy $Pd_{75}Ag_{25}$ single crystals are investigated. The investigated metals have an fcc structure with a lattice constant of 3.89 Å[20] for Pd and 3.84 Å[21] for Rh. According to Vegard's law, the lattice constant, *a,* of an alloy is a linear relationship between the lattice constants of the involved metals, *A* and *B*, and their respective concentrations, *x*.

$$aA_{(1-x)}B_x = (1-x)a_A + xa_B$$

The Vegard's law can be applied to the $Pd_{75}Ag_{25}$ alloy and if Ag is assumed to have a lattice constant of 4.09Å, the resulted lattice constant for the $Pd_{75}Ag_{25}$ alloy is calculated to be 3.94 Å, which is in good agreement of the reported value in the literature of 3.99 Å[22].

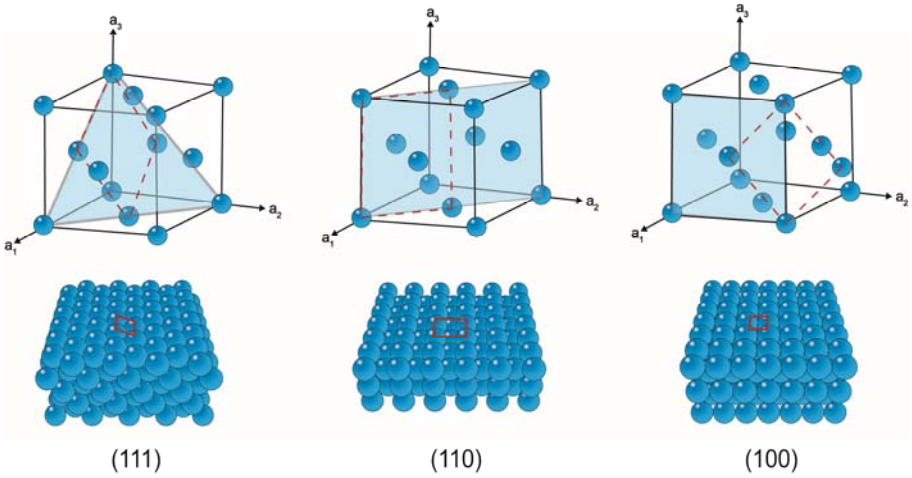

Figure 2:2: The unit cell of the three different low index planes (111), (110) and (100) of an fcc lattice. Model of the surface with the surface unit cell indicated is shown for each surface structure.

The (100) plane has a squared surface unit cell where each atom has eight nearest neighbor atoms that can be compared to twelve for the bulk atoms and is therefore undercoordinated. The properties of the (111) surface orientation are also studied in detail but not as a single crystal but as the facet of the terraces on the vicinal surfaces. The surface atoms in the (111) plane have nine nearest neighbor atoms and are therefore said to be more closed packed surface than the (100) structure, which has only eight nearest neighbor atoms.

2.1.2 Vicinal surfaces

The crystal can be cut in a small angle to a low-index plane resulting in a so-called vicinal surface, because it is "in the vicinity" of the low-index plane. The vicinal surfaces studied in this thesis consist of periodically equally long terraces separated by steps. The width of the terraces and height of the steps is determined by the angle relative to the low-index surface, the crystal is cut in. The terraces, as well as the steps, can be seen as microsurfaces, called facets, which appear as low-index surface orientations. The steps make the surface more complex than the low-index

surfaces, exposing different kind of surface sites. The flat terraces have a low-index surface structure, and on the step edges, undercoordinated atoms are present which mimic the different surface sites on the nanoparticles, making the vicinal surfaces appropriate as model systems[23-25]. The periodicity of vicinal surfaces open up for the use of diffraction-based techniques as well as careful analysis of specific surface sites that are difficult to study at nanoparticles.

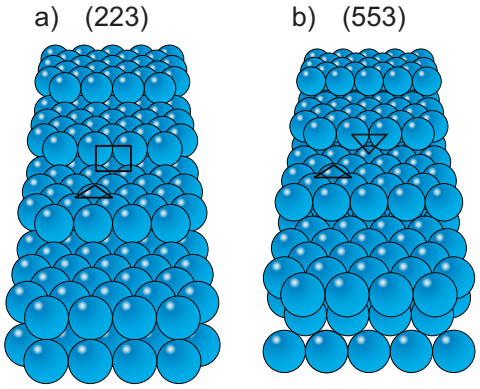

Figure 2:3. Models of the a) (223) surface and b) (553) surface. Both surfaces contain (111) terraces but the (223) surface has steps with the (100) orientation (A-type step) and the (553) surface has (111) orientation (B-type) on the steps.

The steps have also been found to release stress in the surface, arising due to lack of chemical bonds in the topmost atom layer at the surface. The relaxation of the surface often results in a contraction of the atoms at the surface, which is more pronounced on a stepped surface than on an extended low-index surface.

In Paper XIV the vicinal surfaces of (553) and (223) orientation are used as model systems and their surface structures are shown in Figure 2:3. Both surfaces are in the vicinity of the (111) plane and as a consequence, have (111) orientation on the terraces that are five atoms wide. Monoatomic steps separate the terraces, but the step orientation is different for the two surfaces[26, 27]. The (223) surface has {100}-like steps while the (553) surface has {111}-like steps, usually referred to as A- and B-step, respectively.

2.1.3 Cylindrically shaped crystal

Most of the single crystals (vicinal or low-index surfaces) used as model catalysts in this thesis expose a flat surface on the macroscopic scale, but one cylindrically shaped crystal with an "arch-shaped surface" is used. The cylindrically shaped generates a range of different vicinal surfaces, which can be an experimental benefit[28, 29]. In this manner it is possible to compare the behavior of different surface orientations under identical conditions. The cylindrically shaped crystal can also be considered to have several properties similar to the nanoparticles, but it is, in contrast to a nanoparticle, polished such that a well-ordered surface is obtained. The cylindrically shaped crystal used in Paper XIV is made out of Pd and polished around the (111) plane generating vincinal surfaces at an angle up to ±15° relative the [111] direction, see Figure 2:4. This results in a (111) surface orientation on the top of the crystal and stepwise decreasing width of (111) oriented terraces with increasing angle. The terraces are separated by monoatomic {100}-like steps (A-type) in the $[\bar{1}\bar{1}2]$ direction and {111}-like steps (B-type) in the $[11\bar{2}]$ direction. In Paper XIV we show that the steps generate a relaxation, causing an in-plane lattice contraction of the (111) facets at the terraces. The contraction is larger on the terraces with the B-steps, which lower the CO desorption energy. In addition, the relaxation has consequences for the intermolecular repulsion between the adsorbed CO molecules at a high coverage of CO. The result is a lower desorption energy by CO on the terraces, which in turn generates a lower activation temperature for the CO oxidation reaction on the (111) terraces separated by B-type steps compared to the (111) terraces separated by A-type steps.

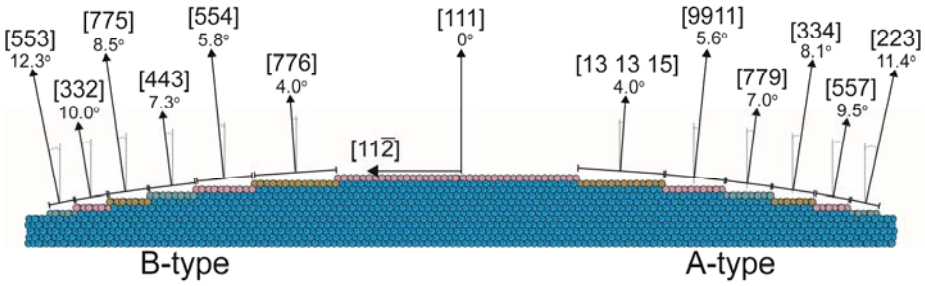

Figure 2:4. A model of the cylindrically shaped crystal polished in the [111] direction generating monoatomic stepped surfaces with decreasing terrace width with increasing angle.

2.1.4 Nanoparticles

A commercial, industrial catalyst is typically made of a powder containing the active material as nanoparticles, which are dispersed throughout an oxide. For investigations of the catalytic activity, the powder can be pressed into a pellet to simplify the practical handling in the experiment. These samples are close to real industrial catalysts, but the complexity of the samples makes it difficult to deduce detailed information about the catalyst surface structure. Therefore, in the present thesis, only gas phase measurements are reported for such samples. In Paper IX pressed powder samples are used to study and visualize the CO_2 distribution above the sample but also to illustrate the potential of studying many catalysts simultaneously. The catalytic powder can also be spread over a monolith, which has a honeycomb-like geometry with the advantage that gas can flow through it. This was utilized when glass tubes were used as flow reactors in Paper IX.

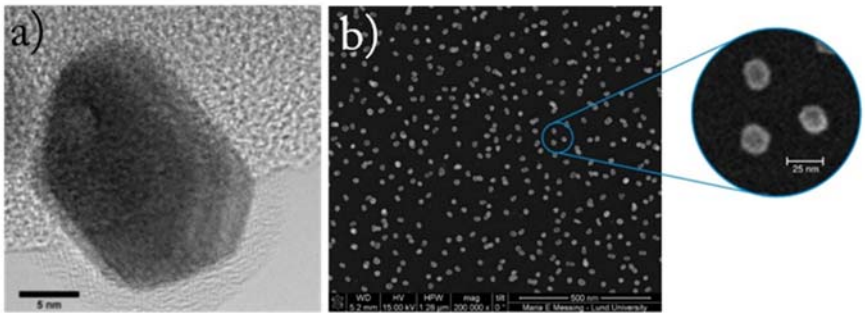

Figure 2:5 a) The TEM image with atomic resolution of a Rh aerosol nanoparticle shows the hexagonal shape of a nanoparticle. b) An overview SEM image indicating that the particles have a similar size and are distributed evenly on the substrate after deposition.

To gain structural information about the surface of particles, catalytic aerosol particles were produced by a spark discharge technique[30]. Using this technique, the particles are size selected and deposited with known coverage on an oxide substrate. The size of the particles were controlled by the use of a differential mobility analyzer (DMA) that classifies the particles according to their charge distribution. The shape of the particles were also controlled in the production by heating the particles in a tube furnace, positioned along the production path. Hexagonally shaped Pd, Rh and PdAg particles, such as the ones shown in Figure 2:5, were generated by this method and studied in this thesis. The well-controlled production of particles makes it possible to produce homogeneous samples, which is an advantage when surface properties are studied by surface science techniques.

The number of techniques capable of providing chemical information of single atoms or molecules is limited, and most often an average signal from a large part of the sample is detected. The evaluation of the raw data is, therefore, simplified if the sample is well defined.

In Papers I, II and V, we study Rh, Pd and $Pd_{25}Ag_{75}$ particles with diameters in the range of 10-30 nm. Previous surface studies suggest that two surface structures, (100) and (111) are dominating a clean catalyst particle,[31-33] exposed to low temperature and pressure, see the model shown in Figure 2:1. The results obtained from the studies of the particles have therefore been compared to results from studies of single crystals with a (100) structure. The comparison allows for studying fundamental differences and similarities between particles and single crystals but also to study size dependent properties of the particles.

2.1.5 Alloy Surfaces

An alloy is a mixture of two or more metals where the aim, in the catalysis area, is to reduce the overall cost of the material while preserving important properties. The bimetallic alloy with the composition of 75% Pd and 25% Ag have been studied both as a (100) single crystal and as nanoparticles in Papers III, IV, V. In these studies, the catalytically active Pd was mixed with the cheaper Ag. The properties of the mixed metals influence the composition of the metals on the surface and segregation effects, depending on the surrounding gas composition, may occur[7, 34]. Previous studies have shown that CO does not adsorb on Ag at room temperature and above and that Ag is inactive in CO oxidation[35]. This is an advantage when fundamental catalytic properties of the alloy of Ag and the less noble metal Pd are investigated. The Ag is also chosen because of the almost matching lattice constant to Pd making the alloying more favorable. Under UHV conditions, Ag is segregating to the surface[36] due to lower surface energy, which is reported to be 0.5 eV/atom less for Ag than for Pd[37]. The segregation is also explained by a stress release caused by the slightly (5%) larger lattice constant for Ag. Theoretical calculations together with experimental results suggest a model of the clean surface where the topmost atomic layer is Ag with a layer of Pd atoms underneath and a mixture ratio of 3:1 of Pd and Ag in the bulk. A model of the $Pd_{75}Ag_{25}(100)$ can be seen in Figure 2:6 together with a model of a Ag(110) surface for comparison. In addition, the Ag $3d_{5/2}$ photoelectron spectra from respectively crystal are shown where the characteristic binding energy shift of -0.72 eV of the Ag bulk component in the alloy as compared to the pure Ag crystal, is indicated.

This shift was used as a fingerprint to identify the $Pd_{75}Ag_{25}$ composition of the samples when the alloy was studied using X-ray photoelectron spectroscopy (the technique is described in section 5.1). The large shift in binding energy of the Ag $3d_{5/2}$ component[38] was also used when the PdAg nanoparticles were characterized. This shift is a good indication of a well-mixed alloyed particle instead of a core-shell structure.

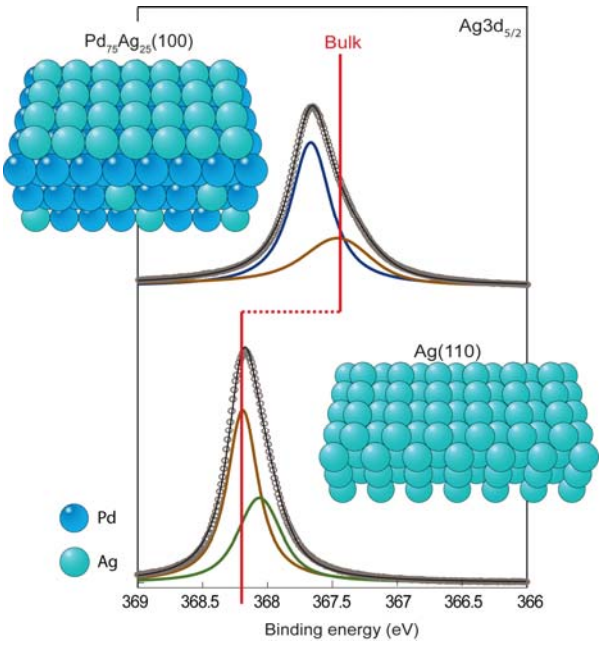

Figure 2:6. A model of clean $Pd_{75}Ag_{25}(100)$ alloy and the corresponding Ag $3d_{5/2}$ photoelectron spectrum (top). For comparison the Ag $3d_{5/2}$ photoelectron spectrum from Ag(110) crystal is shown together with a model of the surface (bottom). A shift of the bulk component of -0.72 eV towards lower binding energy is observed for the alloy as compared to the pure Ag crystal.

3 Surface structures

In the literature, there is a debate whether the oxide or the metal is the most active phase of the Pt-group catalysts in CO oxidation. Both phases have been reported to be experimentally observed during high activity of Pd as well as Rh[39-42]. The knowledge of the oxidation process and oxide structures formed on the catalytic materials is, therefore, crucial for the understanding of the correlation between high activity and the surface structure during a catalytic oxidation reaction.

3.1 Adsorbate induced structures

Gas phase molecules may adsorb on the clean surface where on-top, bridge or hollow are the most common adsorption sites. When the coverage of adsorbates on the surface increases, the adsorbates will arrange in well-ordered structures on the surface. The so-called Wood's notation is often used to describe the structure of the adsorbate. If the surface unit cell is defined by the vectors $\mathbf{a}_1$ and $\mathbf{a}_2$ and the adsorbate by the vectors $\mathbf{c}_1$ and $\mathbf{c}_2$, the unit cell of the adsorbate relative to the unit cell for the clean surface, can expressed as:

$$\left(\frac{\mathbf{c}_1}{\mathbf{a}_1}\times\frac{\mathbf{c}_2}{\mathbf{a}_2}\right)R\alpha$$

where α is the rotational angle between the adsorbate and surface structure. As an example, the chemisorbed oxygen structures illustrated in Figure 3:1, can be considered. With increasing coverage the lateral interaction will cause repulsive interaction between the adsorbates, which prevent adsorption on the nearest neighbor site. The number of occupied adsorption sites on the surface is therefore usually less than the number of substrate surface atoms. The coverage of adsorbates is often given in monolayers (ML), which is defined as the fraction of adsorbates per surface atom.

3.1.1 CO induced structures

In this work, CO is used to study the reduction of oxides or in a mixture with O_2, for the catalytic CO oxidation reaction. Under the conditions used in the experimental studies present in this thesis, the metallic surface is often saturated with CO. A high coverage of CO is detected but a surface reconstruction due to CO adsorption is not observed on any of the studied surfaces. The CO molecule forms a bond with the surface via the carbon atom and adsorbs preferable on the bridge site on Pd(100) and on the three-fold hollow site on Pd(111) resulting in a saturation coverage of 0.75 ML for both surfaces[43-46]. For Rh(100) the CO saturation coverage is reported to be 0.83 ML, which is slightly higher than for Pd(100), a consequence of both bridge and on-top adsorption sites[47]. The saturation coverage of CO on a vicinal surface is influenced by the presence of steps on the surface. The intermolecular repulsion between the CO molecules is more pronounced at the terraces-step border, which influences the total CO coverage on the surface. The step orientation also affect the CO coverage on the vicinal surfaces, as discussed in Paper XIV. When CO is used to study the reduction of the oxides, our results indicate that CO adsorbs on the undercoordinated atoms in the PdO(101) bulk oxide. For the Rh oxides, the CO is most probably adsorbed on defects in the oxide[48], and the reduction process proceeds via reduced islands, as discussed in Papers I, II and IV.

3.1.2 Chemisorbed oxygen structures

Stable chemisorbed oxygen structures are formed on the Pd(100) surface starting with the lowest coverage of 0.25 ML in a p(2×2) structure followed by a c(2×2) formation at a coverage by 0.5 ML, shown in Figure 3:1. An additional (5×5) oxygen induced structure has been reported for coverage of 0.7 ML but with an unknown structure[49-51].

A p(2×2) structure, with oxygen in four-fold hollow sites, is also observed on Rh(100) at a coverage of 0.25 ML. The Rh surface, however, reconstructs at higher oxygen pressures and the surface reveals more energetically favorable three-fold hollow adsorption site for oxygen. At 0.5 ML and 0.67 ML coverage the oxygen forms (2×2)pg-2O and (3×1) structures, respectively,[52-54] also observed in Paper VII under reaction conditions.

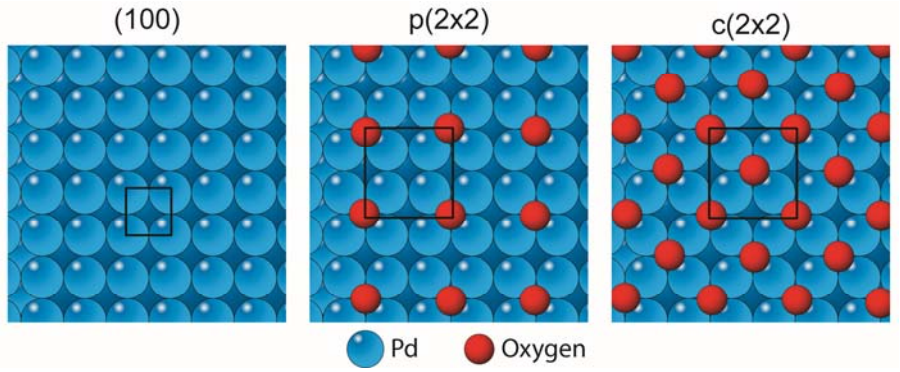

Figure 3:1 Models of the different chemisorbed oxygen structures on Pd(100), where the different unit cells are indicated.

Oxygen exposure of a vicinal surface results in a more complicated oxidation picture of the surface than on the low-index surfaces. The oxidation process of the stepped (553) surface, for example, start with oxygen atoms decorating only the step edges. Further oxidation generates oxygen adsorption also on the terraces followed by a reconstruction of the surface at higher oxygen exposure. The reconstructed Rh(553) surface contains (111) and (331) facets[27] while the reconstruction of Pd(553) is more complex with (332) facets dominating the surface but coexisting with (221), (775) and (110) facets[26]. Turning to the vicinal surfaces with A-type step such as (223), the Rh(223) surface transform to facets with (113) and (111) orientation[55] while the Pd(223) surface reconstruct to (211) and (111) facets before the surface oxide is formed.

3.1.3 Surface oxides

The theoretical predictions of stable phases are calculated using density functional theory (DFT), and according to thermodynamics, the surface will start to incorporate oxygen atoms when the energy gained to form an oxide is higher than the energy cost of removing an oxygen molecule from the gas phase. If the oxygen only mixes with the first atomic metal layer, it is referred to as a surface oxide. If the mixture occurs deeper into the crystal, a bulk oxide is formed.

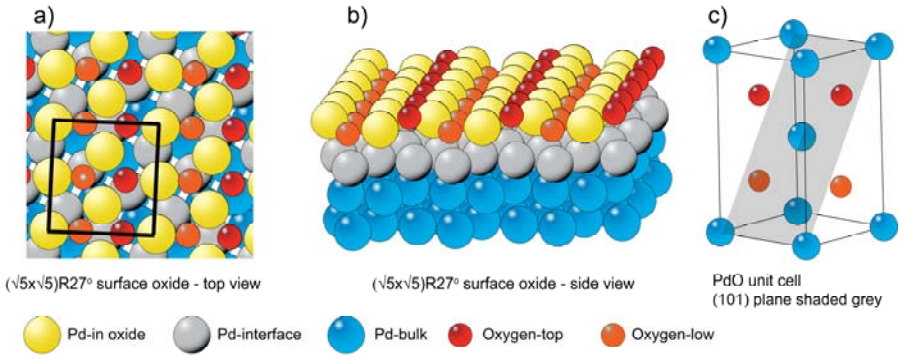

Figure 3:2. a) A model of the (√5×√5)R27°- oxide in where the surface unit cell is indicated. b) a side view of the surface oxide. c) The PdO unit cell is shown where the (101) plane is shaded grey. The PdO is suggested to grow in the (101) direction on the Pd(100) and the surface structure of the PdO(101) is almost identical to the surface oxide.

It has been found, both through experiments[20, 50, 56-60] and calculations[20], that the surface oxide with a (√5×√5)R27° surface periodicity is stable over a wide pressure and temperature range on the Pd(100) crystal. This 2D oxide has an oxygen coverage of 0.8 ML and consists of a single PdO(101) plane on top of the Pd(100) substrate[50]. In the oxide layer, the Pd atoms are coordinated to two or four oxygen atoms respectively with every second row of oxygen located slightly above the Pd atoms (0.6 Å) and every second row is approximately 0.4 Å below the Pd atoms[57]. A similar effect can be seen on the Pd atoms positioned at a hollow and bridge sites where the fourfold Pd atoms are slightly higher than the twofold Pd atoms.

The bulk oxide on Pd(100) has been considered to expose three different surface orientations, PdO(001), PdO(100) and PdO(101). From the thermodynamical point of view, PdO(100) has the lowest surface energy[61, 62]. However, the PdO(101) has been reported to be the energetically most favorable growth and surface orientation due to the small mismatch between the oxide film and substrate[50, 57, 61]. In Paper I we observe the PdO(101) surface orientation of the bulk oxide. Shown in Figure 3:2c) is the unit cell of PdO, and a cut along the (101) plane will generate a surface unit cell with a size of 6.13 Å × 3.03 Å[57]. In the PdO bulk, each Pd atom binds to four oxygen atoms, however, the (101) surface termination results in three-fold oxygen coordinated Pd atoms. As in the surface oxide, every second row of the oxygen will be located slightly above or below the Pd atoms.

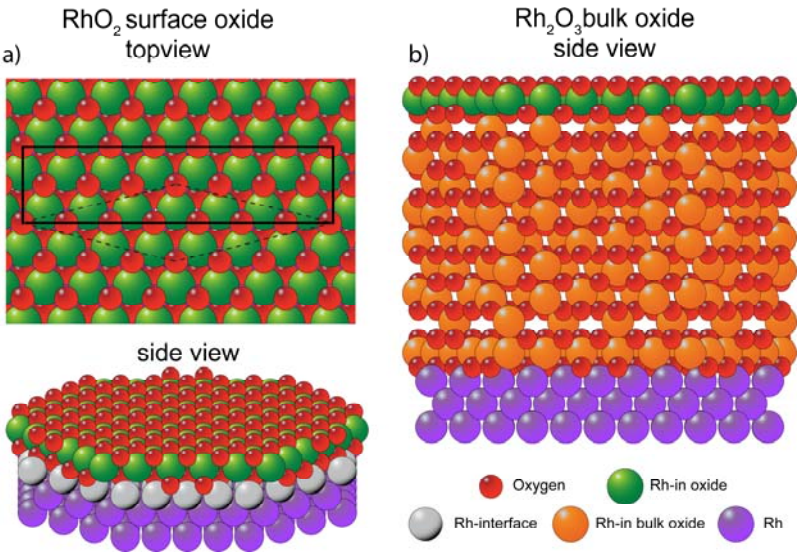

Figure 3:3 a) Top view and side view of the trilayer surface oxide. The (8x2) surface unit cell as well as the c(8x2) unit cell (dashed lines) are indicated in the top view model. b) Side view of the Rh bulk oxide grown on the Rh(100) with a trilayer terminated surface. The model illustrates the denser structure in the trilayer compared to the Rh underneath.

The Rh surface oxide has a trilayer structure consisting of two oxygen layers separated by a Rh layer (O-Rh-O) (see Figure 3:3a) and has been observed on all investigated surfaces as well as on Rh particles [27, 31, 33]. The hexagonal *c*(8×2) oxide structure of RhO_2 on Rh(100) has a lattice constant of 3.07 Å and corresponds to an oxygen coverage of 1.75 ML on the surface[63]. The interface oxygen atom layer between the substrate and the *c*(8×2) structure is positioned in on-top and bridge site on the Rh(100). The next atomic layer is Rh where each metal atom binds to six oxygen atoms. The top most layer is an additional oxygen layer resulting in an oxygen covered surface with no undercoordinated Rh atoms as opposed to some of the Pd atoms in Pd surface oxide.

The Rh surface oxide is often detected experimentally although it is only thermodynamically stable over a narrow range of chemical potentials. This is because the surface oxide has been shown to hinder oxygen to incorporate in the Rh metal and form a bulk oxide. The bulk oxide of Rh has a Rh_2O_3 termination with a hexagonal structure in the (0001) direction and a lattice constant of 5.21 Å[64]. It has been shown that the surface of the bulk oxide also exposes a trilayer structure similar to the surface oxide[65].

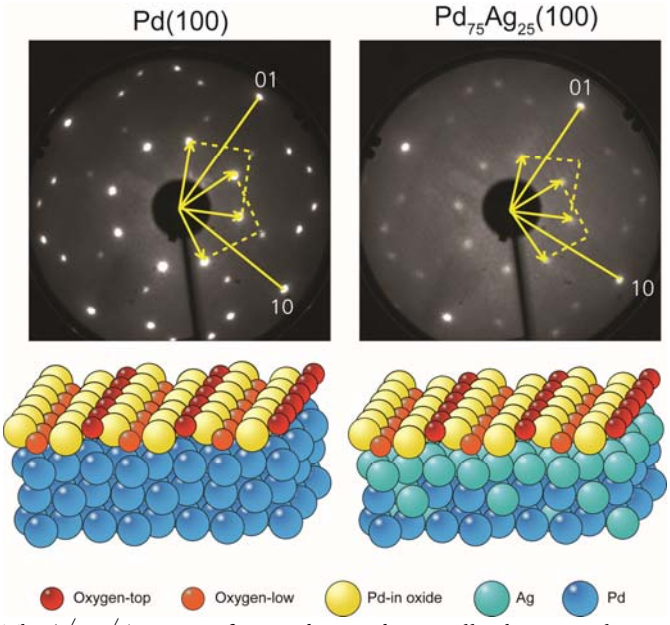

Figure 3:4 The (√5×√5)R27° surface oxide on $Pd_{75}Ag_{25}$ alloy has a similar structure as the surface oxide observed on the pure Pd(100). Models of the surface oxide formed on the Pd(100) and $Pd_{75}Ag_{25}$(100) together with the corresponding observed LEED pattern, are shown for each surface. The LEED images recorded after exposing the crystals to oxygen, reveal a similar pattern indicating that a surface with the same periodicity is formed on both crystals. The (√5×√5)R27° unit cell is shown in yellow in the LEED pattern.

The surface reconstruction, of the bulk oxide forming a trilayer structure on topmost atom layers, results in a 50% denser Rh layer in the surface than the bulk oxide structure. Consequently, the second Rh layer is 50% less dense as illustrated in Figure 3:3b). The trilayer surface oxide, as well as the bulk oxide, is observed in the oxidation characterization of Rh in Paper II.

Exposing the $Pd_{75}Ag_{25}$ alloy to oxygen, studied in Paper III and V, results in a segregation of the Pd to the surface[66] where it reacts with the oxygen and forms a surface oxide. Interestingly, a (√5×√5)R27° surface oxide with a similar structure as on Pd(100) is also formed on the $Pd_{75}Ag_{25}$, see Figure 3:4, but the mismatch between the substrate and the oxide is slightly larger for the $Pd_{75}Ag_{25}$(100) than for the Pd(100) becauce of the larger lattice constant for the alloy. One important difference from the Pd(100) is the interface between the substrate and surface oxide, which consists of an almost complete Ag layer for the alloy. This Ag layer may inhibit further oxidation forming a bulk oxide, which never is observed under the conditions studied in this thesis.

4 Heterogeneous catalysis

In a heterogeneous catalytic reaction the reactants and the catalyst are in different phases. Usually, the catalyst is a solid and the reactants are in gas phase or liquid phase. The catalytic reaction occurs, in this case, on the surface of the catalyst and are often not fully understood. To increase the knowledge about the chemical process, a more complete picture of the reaction is needed. A major part of the chemical process is the interaction between the surface and the surrounding gas phase. It is, therefore, essential to study both the surface structure and the gas distribution in the vicinity of the catalyst, ideally simultaneously. During a catalytic reaction, the gas composition is changing with the activation of the catalyst, and *operando* studies should therefore be performed.

4.1 Reactivity of transition metals

The transition metals are also called *d*-block elements due to their partly filled *d*-band. The number of electrons in the *d*-band have a significant impact on the reactivity of the metals, which can be explained by the *d*-band model[67]. The number of electrons in the *d*-band increases towards the right in the periodic table and as a result the electrons are more delocalized to the individual atoms generating an increased width of the *d*-band. This generates a shift of the center of the *d*-band, down from the Fermi level. An increasing periodic number (down in the periodic table) also shifts the *d*-band down in energy due to an increasing overlap of the wave functions, which broaden the *d*-band as illustrated in Figure 4:1a). A *d*-band located close to the Fermi level results, according to the *d*-band model, in high reactivity of the metal.

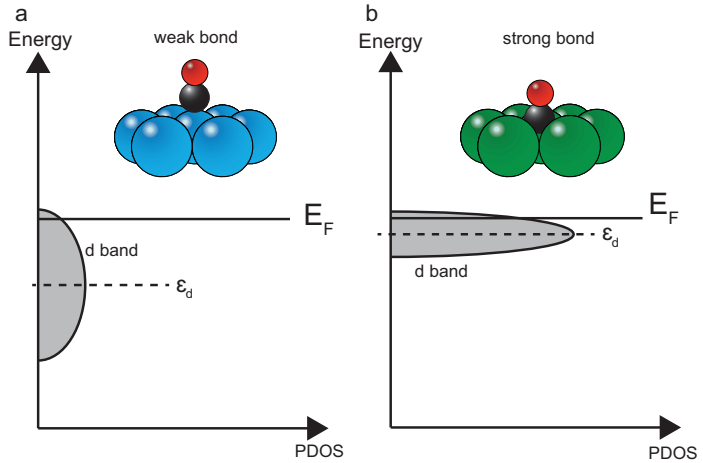

Figure 4:1 Schematic illustration of the projected density of states (PDOS) in the d-band that influence the strength of the interaction between a molecule (CO) and the surface. a) The transition metals to the right in the periodic table have the centre of the d-band shifted down from Fermi level. This generate a weak interaction with adsorbates, illustrated as a weakly bonded CO molecule on the surface in the figure. b) A narrow d-band with a centre close to the Fermi level generates a reactive surface, illustrated as a CO molecule that is strongly interacting with the surface.

Open surfaces, which in common with steps and kinks, contain undercoordinated atoms results in a narrow *d*-band close to the Fermi level, illustrated in Figure 4:1b). The position of the *d*-band generates a strong (or weak) interaction between an adsorbate and the *d*-band of the metal, resulting in a splitting of the adsorbate's energy levels into a bonding and an antibonding state. The strength of the chemisorption is increased by the population of electrons in the antibonding state but in turn the internal bonding of the adsorbed molecule is weakened[68]. These undercoordinated adsorption sites are widely discussed in the literature, to be the most important sites on the surface for some catalytic reactions[69-72]. According to the Sabatier principle, the interaction between the surface and the adsorbate should be of just the right magnitude – not too strong and not too weak. This will generate an efficient catalyst. If CO oxidation is considered, the adsorption of the O_2 molecule should result in dissociation followed by a reaction of an adsorbed CO molecule. Hence, it is important that the adsorption of CO does not result in a dissociation on the catalyst. The adsorption energy of CO is lower than for the dissociated O atom[73], making the CO more mobile and the CO may diffuse on the surface to react with an adsorbed O atom. The adsorption of the resulting CO_2 molecule should be weak resulting in desorption from the surface.

4.2 CO oxidation

In a catalyzed CO oxidation reaction, the adsorption and desorption processes of the reactants are surprisingly complex. The aim of the reaction is to produce CO_2 of the two reactants O_2 and CO as described below.

$$2CO + O_2 \rightarrow 2CO_2$$

In general, three different mechanisms, Langmuir-Hinshelwood, Mars-van Krevelen and Eley-Rideal, are used to describe the CO oxidation reaction, and the Langmuir-Hinshelwood mechanism is the most common one. In the Langmuir-Hinshelwood mechanism, the CO oxidation is believed to occur via adsorption of CO and O_2 on the surface where O_2 adsorb dissociatively (step 1 and 2 below). CO and O can subsequently react (step 3) and desorb from the surface as CO_2 (step 4). This can be described in the four reaction steps shown below:

$$(1)\ CO_g + * \rightleftarrows CO^*$$
$$(2)\ O_{2_g} + 2* \rightleftarrows 2O^*$$
$$(3)\ CO^* + O^* \rightleftarrows CO_2 + *$$
$$(4)\ CO_2^* \rightleftarrows CO_{2_g}$$

where *g* denote the gas phase and * an available surface site. This mechanism is reported for CO oxidation on Pd(100) by Chen *et al.*[74], but also on Pd(111) by Engel *et al*[75].

Another suggested mechanism for CO oxidation is the so-called Mars-van Krevelen mechanism. This reaction proceeds via an oxidized catalyst surface that interacts with the reactants in the gas phase. The mechanism will, therefore, require oxidizing conditions for the catalyst surface, which usually implies high partial pressure of oxygen. In the Mars-van Krevelen mechanism, in contrast to Langmuir-Hinshelwood, the adsorbed oxygen should react with the metal and form at least a surface oxide on the surface. In CO oxidation, the Mars-van Krevelen process will proceed via an adsorbed CO molecule, which reacts with an oxygen atom in the oxide, leaving the surface as CO_2 and an oxygen vacancy remaining on the surface. An oxygen atom from an O_2 molecule that adsorbs dissociatively on the surface fills this vacancy and reforms the oxide. CO oxidation is reported to occur on an oxidized Pd(100) surface via the Mars-van Krevelen mechanism by Hendrikssen *et al.*[76] and

by Onderwaater *et al.*[77]. The mechanism is also suggested for the CO oxidation on RuO_2(110) by Over *et al.*[40].

In the Eley-Rideal mechanism, only one of the reactants is adsorbed on the surface, while the other reactant, in the gas phase, will approach and react with the adsorbed reactant but without adsorbing itself. Toyoshima *et al.* [78] propose that CO oxidation proceeds via the Rideal-Eley mechanism on the three-fold coordinated oxygen atoms in a Pd_5O_4 oxide (surface oxide on Pd(111). The Rideal-Eley mechanism was also suggested to be the most favorable reaction for a PdO(101) surface by Hirvi *et al.* [79]. Illustrations of the three different reactions can be seen in Figure 4:2.

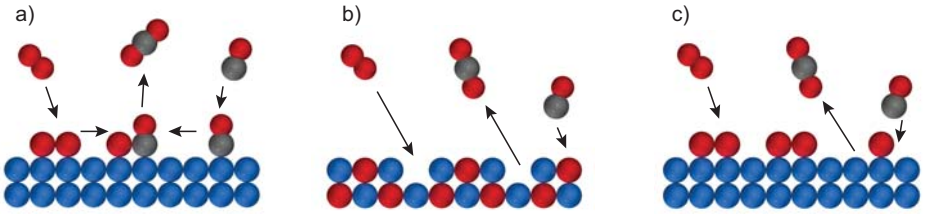

Figure 4:2 Three different reaction mechanisms suggested for the CO oxidation. a) Langmuir-Hinshelwood b) Mars-van Krevelen and c) Eley-Rideal.

4.3 The change of the gas composition during the catalytic reaction

The CO oxidation process can proceed via catalyzed or uncatalyzed pathways, where the main difference will be the activation energy, ΔE of the reaction. This is the energy barrier that the reaction has to overcome to occur. The correlation between production rate and the activation energy was first described by Svante Arrhenius, for which he later was awarded the noble prize. The Arrhenius equation is written as:

$$k(T) = Ze^{-\frac{\Delta E}{k_B T}}$$

where k is the rate constant, Z is the prefactor; k_B is the Boltzmann constant and T, the temperature. The prefactor is a constant that contains information about the number of collisions that occur between the surface and the gas molecules.

The Arrhenius equation shows that the rate of the reaction has an exponential dependence on the activation energy and temperature, which implies that the rate of a reaction will increase significantly if the potential barrier of the reaction is reduced or if the temperature is increased. In all *operando* experiments performed in this work the temperature of the catalyst is increased in a gas mixture of CO and O_2. The studies in this thesis show that at the beginning of the experiment, CO saturates the surface on the cold catalyst resulting in CO poisoning. The reaction rate is then close to zero because the CO inhibit the O_2 dissociation by blocking dissociation sites. By increasing the temperature, a gradually increase in the activity is observed, which is correlated to the desorption of the CO molecules. During this temperature interval the reaction rate follow the Arrhenius expression mentioned above, and the activation energy for the reaction can therefore be calculated. When the surface reaches the temperature where all adsorb CO can react with the oxygen on the surface, the catalyst becomes extremely efficient in the CO oxidation process and the reaction rate increase significantly, which is observed as a sudden increase in the CO_2 production. This temperature is referred to as the light-off temperature, the activation temperature, or the ignition of the reaction. Before the light-off, the CO oxidation process is strongly dependent on the CO desorption, which is the rate limiting step in the process under these conditions. The light-off temperatures for Pd(100) and Rh(100) was studied in Paper VI and VII, where we found an increasing light-off temperature and oxygen coverage on the surface immediately after light-off with increasing total pressure (at a 1:1 ratio of CO and O_2). The increased light-off temperature can be explained by a shorter lifetime of a vacant surface site due to the increased number of gas-surface collision with higher pressure. For the cylindrically shaped Pd(111) crystal studied in Paper XIV, different light-off temperatures were detected at different parts of the surface, which is correlated to the different step orientations.

After light-off, the catalyst is highly active, and for CO oxidation the exponential dependency of the temperature and energy barrier is no longer valid. The reaction rate is instead controlled by the diffusion of the reactants to the surface and is said to be mass transfer limited (MTL) by a reactant. This means that all molecules of the minority reactant (CO in the cases studied in this thesis) that reach the catalyst are converted into the product. A gradient of the reactant concentration close to the catalyst is created in this regime, and the total gas composition close to the catalyst is, therefore, different as compared to the gas composition at the inlet or outlet of the reactor[80]. This has a significant impact on the surface structure, which will change depending on the interacting gas molecules. The strong oxidizing environment close to the surface in the MTL regime, may therefore results in an oxide formation. This

has resulted in a lively debate in the literature whether the oxides found in the highly active and MTL regime also is the most active phase of the catalyst. It has been reported that the high activity in CO oxidation for the oxidized Ru, is associated to the undercoordinated atoms in the $RuO_2(110)$ surface[40]. The undercoordinated atoms in the PdO(101) are suggested to work as the active sites during CO oxidation[81]. In this work the most active site has not been investigated but in Paper VI and VII we report on a chemisorbed oxygen structure present on both Pd(100) and Rh(100) in the highly active regime when the crystals are exposed to a 1:1 ratio of CO and O_2 up to 1 Torr and temperatures up to 450°C. To confirm that also the oxide can be present in the highly active regime, the Pd surface has to be exposed to a 1:4 ratio of CO and O_2. An oxide is never observed during catalytic CO oxidation over Rh(100) in this study. The lack of the surface oxide indicates that at a total pressure of 1 Torr the partial pressure of O_2 in the highly active regime is too low (or the CO partial pressure is still too high) to oxidize the surface. In a higher total pressure and thereby more realistic conditions, we expect a surface oxide in the 1:1 ratio on both Pd and Rh.

The PdO with a (100) structure, on the other hand, is oxygen terminated and does not expose any undercoordinated atoms. This is also true for the surface oxide and the bulk oxide on the Rh, which is considered to be less active even though a surface oxide often is detected on Rh(100) in the MTL regime [82, 83]. This observation can be explained by reduced areas on the surface, exposing the active metal site, which is due to the exponential dependence of the reaction rate, enough to keep the reaction in the MTL regime. The same scenario is also suggested for the most active phase of Pd(100) discussed in Paper XII.

Further, not only the onset of a catalytic reaction may affect the surface structure, but also the flow configuration and geometry of the reactor in which the experiments are performed. This is discussed in more detail in chapter 5.2.

5 Experimental methods

In this work, we have used Ambient Pressure X-ray Photoelectron Spectroscopy (APXPS) for surface and gas-phase studies and Planar Laser-induced Fluorescence (PLIF) for gas phase visualization. APXPS has been used to perform *in situ* studies of the surface chemical composition during oxidation by O_2, reduction by CO and during the catalytic oxidation of CO. The pressure conditions during which the surface is studied with APXPS (10^{-6} – 1.3 mbar) is closer to realistic conditions of a catalyst than what can be achieved in common UHV chambers. The high-pressure studies have generated questions about the influence of the active catalyst on surrounding gas phase of the catalyst. We have therefore used Planar Laser Induced Fluorescence (PLIF) to study the CO_2 and CO gas phase above the catalytic active surface during CO oxidation. In this chapter the two methods above is discussed. Further, additional experimental techniques necessary for the interpretation of the data obtained under *operando* conditions will also be described.

5.1 X-ray Photoelectron Spectroscopy

Photoelectron spectroscopy is based on the theory of the photoelectric effect, first described by Einstein in 1905[84], for which he was rewarded the Nobel Prize in physics 1921. An atom can be ionized when irradiated by X-rays, knocking out a core electron. The emitted core-electron, called photoelectron, is detected, and the corresponding binding energy of the photoelectron can then be determined if the photon energy is known. The binding energy acts as a fingerprint of the specific element and often also its chemical surroundings. During the 1950s, K. Siegbahn *et al.* developed a spectrometer combined with an X-ray source that led to the first X-ray Photoelectron Spectroscopy experimental setup, and in 1981 he received the Nobel Prize in physics for his work in this field[85]. Siegbahn called the technique Electron Spectroscopy for Chemical Analysis (ESCA), and a large number of gas molecules, as well as surface structures, were investigated during the 60s'[85]. In the following decades, the development of the technique progressed in the direction of

decreasing the pressure in the experimental chamber to achieve better statistics of the detected photoelectron spectrum from the surface. As a result, high-resolution binding energy spectra from a surface could be achieved. This technique has since then been further developed, and gas phase detection using XPS was revitalized in the 90s' when an increased interest for *in situ* reaction measurements arose. The technique operating at reaction conditions is referred to as high pressure (HP-), ambient pressure (AP-) or near ambient pressure (NAP-) XPS.

5.1.1 Principle of operation

Photons originating from a synchrotron or an X-ray lab source have enough energy to ionize an atom or molecule. The relation between the kinetic energy, *KE*, of the detected photoelectrons and the binding energy, *BE*, can be described as

$$BE = h\nu - KE - \Phi_{spec}$$

where h is the Planck's constant, ν is the frequency of the incoming light, and Φ_{spec} is the work function of the spectrometer. The work function is the minimum energy required to remove an electron from the surface. The conducting sample and the spectrometer are connected to the same ground which aligns their Fermi levels, and the final barrier the electrons have to overcome to reach the analyzer is the vacuum level of the spectrometer. A schematic figure of the energy levels involved can be seen in Figure 5:3. For the transition metals Pd and Rh, the $3d$ is the energy level with the highest cross sections for electron emission. The electrons emitted from the $3d$ energy level will give rise to two peaks in the photoelectron spectrum, see Figure 5:1a). The splitting of the two peaks is called the spin-orbit splitting and is a result from different total angular momentum $j=l\pm s$ of the detected electrons, which is 2±½ for the *d* energy level. The intensity ratio of the spin-orbit doublet peaks is related to the multiplicity $(2j+1)$ of the levels. Thus, the intensity ratio between the splitting of the *d* electrons is 3:2.

The photoelectrons emitted from a clean surface may give rise to two peaks in the spectrum, which can be assigned to electrons originating from the bulk and the surface atoms. The atoms in the topmost atomic layer at the surface lack neighbouring atoms on the vacuum side of the surface and as a result, the photoelectrons emitted from these atoms appear at the lower binding energy side in the spectrum.

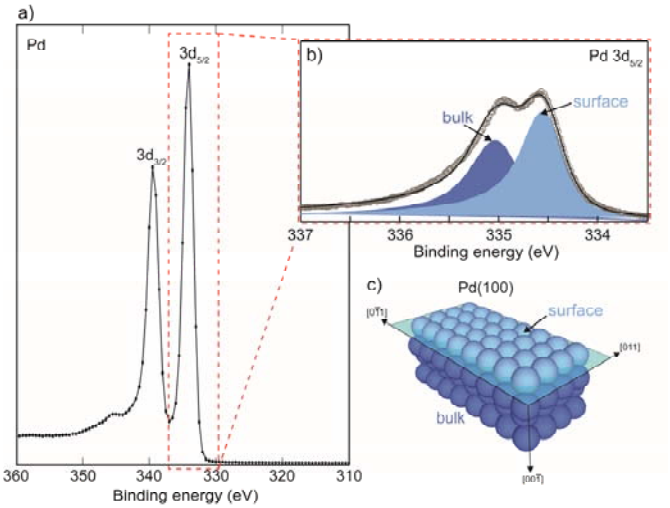

Figure 5:1a) The spin-orbit split of the Pd 3d energy level. b) The Pd3d$_{5/2}$ photoelectron peak, which can be decomposed into two components, one originating from the surface (light blue) and one from the bulk (dark blue). c) A model of the Pd(100) surface.

The possibilities to distinguish between the surface and the bulk in the spectrum is illustrated in Figure 5:1b), which shows a photoelectron spectrum with electrons emitted from a clean Pd(100) surface, illustrated in Figure 5:1c).

The mean-free-path of the emitted electrons is determined by their kinetic energy. The photon energy range used in standard XPS results in a kinetic energy of the electrons that generates a very short mean-free-path. As a consequence, XPS is sensitive to the very first atomic layers at the surface, and therefore a powerful tool for surface studies. The kinetic energy of the photo electrons can be varied by varying the photon energy of the incoming light. In this way, it is possible to achieve a depth profile of the surface. This is performed in Papers I, II, V, VI, and VII, to characterize the surfaces. When photon energy dependent measurements are performed, it is important to make a careful analysis of the spectra, to rule out photoelectron diffraction effects that may influence the detected intensity of the photoelectron peaks[86]. Diffraction of the photoelectrons emitted from neighbouring atoms may occur and constructive interference of the electrons will enhance the intensity of the detected photoelectron peak. The diffraction effect is therefore strongly dependent on the detection angle and photon energy.

5.1.2 Spectrum Deconvolution

The natural linewidth of the photoemission spectrum is determined by the lifetime, τ, of the core hole, which is referred to as the time it takes before the core hole is filled by another electron. The spectrum has a Lorentzian line shape, and the Heisenberg uncertainty principle limits the FWHM (full width half maximum) according to

$$\Delta E_n = \frac{h}{\tau}$$

This contributes to a larger FWHM for photoelectrons emitted from an *s* shell than electrons emitted from a *d* shell, due to the lower probability of filling up the core-hole in a *d* shell than in an *s* shell. The instrumental broadening of the spectral peak has a Gaussian line shape where the analyzer plays an important role for the spectral resolution. The analyzer consists of two hemispheres where the applied potential between the two spheres states the pass energy, E_p. The pass energy, defines the kinetic energy of the photoelectrons that can pass the hemisphere to the spectrometer without colliding with the walls in the sphere. The resolution of the analyzer is given by

$$\frac{\Delta E}{E_p} = \frac{w}{R_{sphere}} + \frac{\alpha^2}{2}$$

where R is the mean radius of the hemisphere, w is the width of the entrance slit, and α is the half angle of the analyzer. As can be seen from the expression above, the resolution is inversely proportional to the radius of the analyzer, and the resolution can therefore be improved by increasing the radius of the hemisphere but also by decreasing the pass energy. The hemisphere is working at a constant pass energy, which has the advantage that the resolution is the same for all kinetic energies. By adjusting the applied voltage to the lenses that control the reacceleration of the electrons before entering the hemisphere, it is possible to detect electrons with different kinetic energy. The number of electrons that pass the hemisphere and are detected, reflect the intensity of the photoelectron peak in the spectra. The statistics in the spectra can be improved by using a light source with high photon flux, such as a synchrotron.

The detected photoelectron spectrum is deconvoluted in the analysis process to interpret the data. The fitted peaks have mixed Lorentzian and Gaussian line shapes, but the transition metals have a pronounced asymmetry that has to be taken into account. The asymmetry of the peak is a result of inelastically scattered electrons.

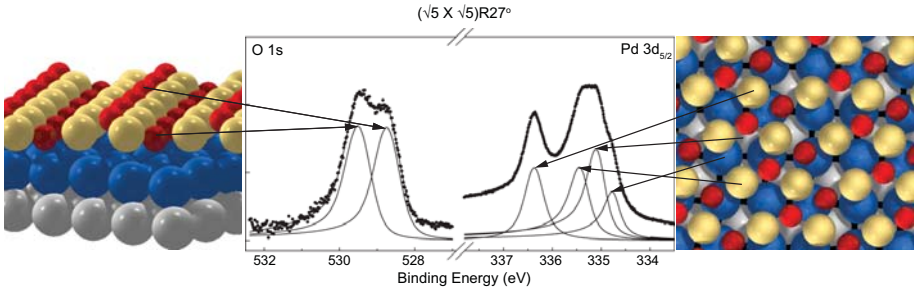

Figure 5:2 The O1s and Pd $3d_{5/2}$ photoemission spectra are shown together with the corresponding top view model of the(√5×√5)-R27° oxide to the right and a side view to the left. Indicated are also the four- and two folded Pd atoms demonstrating that the binding energy of the electrons from Pd is increasing with increasing oxygen coordination. A similar trend can be observed for the oxygen spectrum.

This effect is an intrinsic energy loss process and will be most strongly pronounced in *d*-metals, due to the high density of states near the Fermi level. A Lorentzian with an asymmetric line shape is called Doniach- Šunjić after the scientists that developed it[87]. In this thesis, the spectra are fitted with a Doniach-Sunjic line shape convoluted with a Gaussian.

The binding energies of the core electrons are influenced by the bonding of the valence electrons and the chemical composition. In Figure 5:2 a high-resolution spectrum of the Pd $3d_{5/2}$ energy level is shown measured from a surface oxide on a Pd(100) single crystal. After subtraction of a linear background, the raw data is fitted with four components according to the line shapes described above. The model of the (√5×√5)-R27° surface oxide is shown in Figure 5:2. The four components in the Pd $3d_{5/2}$ spectrum, all originating from Pd, have different binding energies related to differences in their chemical surroundings. The shift in binding energy due to the chemical surrounding is called a *chemical shift*. The observed chemical shift can be interpreted as an initial state effect and correlates to the degree of oxidation of the Pd. The net extra positive charge at the Pd atom because of the bonding with oxygen, will cause a more strongly bound core electron and therefore appear at a higher binding energy in the photoemission spectrum. The most shifted peak can, therefore, be assigned to Pd atoms binding to four oxygen atoms and the second most shifted component to Pd atoms binding to two oxygen atoms. When the surface oxide is formed, the distance between the PdO layer and the substrate increases and is almost decoupled from the Pd atoms at the interface layer. The binding energy of the interface Pd atoms will, therefore, have a surrounding more

similar to the clean Pd surface atoms, and a small negative binding energy shift relative to the bulk is observed.

This simplified model of explaining the binding energy of chemical shifts is a good approximation but since the binding energy is defined as the difference in total energy between the initial state (the ground state) and the final state (the core ionized state) relaxation and screening of the core ionized state should be taken into account. This is not done in the above initial state interpretation of the Pd spectrum, and therefore some care should be taken using initial state interpretations. The situation is delicate, since the final state effect on the binding energy depends on the initial state, thus the two states are entangled. To predict chemical shifts, ab-initio calculations of binding energies, including both initial and final states with a core hole should be performed.

5.1.3 Ambient Pressure X-ray Photoelectron Spectroscopy under semi-realistic reaction conditions

Today, the XPS is developing in the direction of fulfilling Siegbahn's initial vision of probing the gas phase and the surface chemical composition simultaneously. 60 years of improvements[88, 89] from the first experimental setup has made APXPS to a frequently used technique by scientists investigating catalytic reactions *operando*[90]. In this thesis, operando studies of the catalytic reaction of CO oxidation has been performed where the surface chemical composition, as well as the gas phase, are probed. One advantage of *operando* studies is the possibility of detecting and studying the gas phase close to the surface during the reaction, revealing information that cannot be observed by the mass spectrometer (MS) that usually detect gas molecules much further away from the surface[91].

As a rule of thumb, the photoelectrons from gas phase molecules are detected at higher binding energy as compared to the same molecule adsorbed on the surface. Gas phase peaks are therefore usually easy to separate from surface related peaks. The binding energy of the gas phase core level electrons are not referenced to the Fermi level of the sample as is done for the electrons originating from the surface. Instead the ionization energy of gas phase molecules should be referenced to the vacuum level of the gas[92]. The vacuum level of the gas is determined by the electrostatic field between sample and aperture, which is strongly affected by their work functions, as illustrated in Figure 5:3. This effect can be used to determine the work function of the sample, which is strongly influenced by chemical reactions at the surface[93].

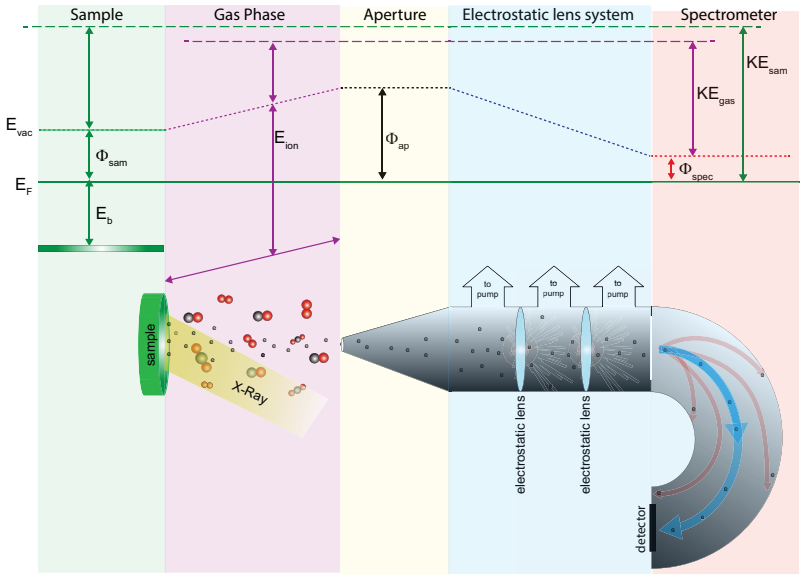

Figure 5:3 Illustration of the energy barriers relevant for APXPS. The kinetic energy, KE, of the photoelectrons from the surface and gas phase are detected, and the binding energy, E_b, can thereby be determined which is referenced to the Fermi level, E_F. The ionization energy of the gas phase molecules, E_{ion}, will change with the work function of the sample, Φ_{sam}. The APXPS setup is equipped with electrostatic lenses with pumping stages in between to maximize the number of electrons in the hemisphere and detector.

The C 1s spectrum in Figure 5:4, recorded during CO oxidation over Pd(100), is an example where the CO and CO_2 gas phase peaks are located at higher binding energy (>290 eV) than the CO adsorbed on the surface at 286 eV. At 335°C the CO_2 gas phase peak is detected indicating that the sample is active in the CO oxidation reaction, illustrating the usefulness of the capability to detect the gas phase. A surprising observation is that no CO can be detected either in the gas phase or on the surface after light-off. This behaviour is discussed in more detail in section 5.2.

The surrounding gas attenuates the number of photoelectrons detected from the surface significantly due to the short mean-free-path of electrons. Electrons with a mean-free-path of 1 nm in a solid would have a mean-free-path of about 1 mm at a gas pressure of 1 mbar, which implies that the detector has to be positioned close to the surface.

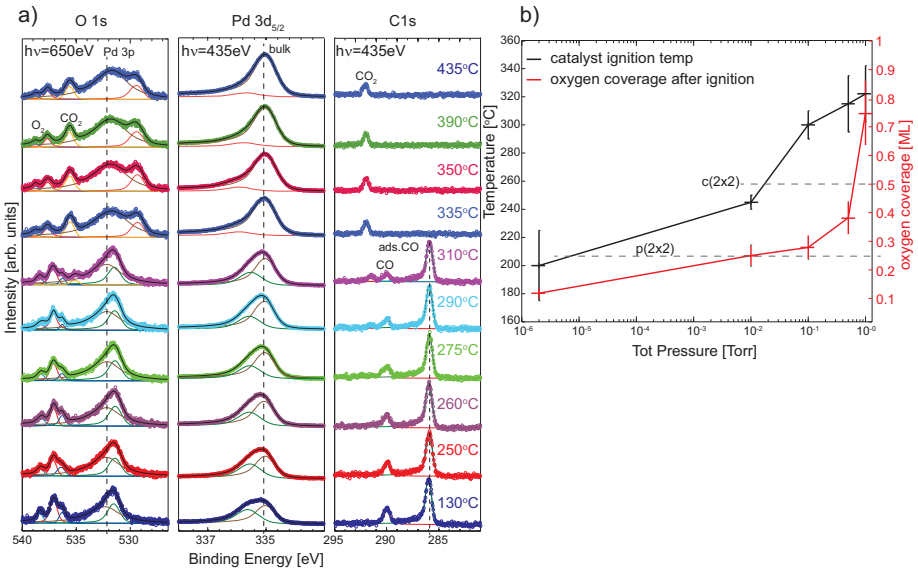

Figure 5:4. The CO oxidation over Pd(100). a) The APXPS spectra detected at 0.25 mbar CO and 0.25 mbar O_2. The O 1s, Pd $3d_{5/2}$ and C 1s spectra were recorded at each temperature indicated to the right in the C 1s spectra. Between 310°C and 335°C the sample becomes active. b) The light-off temperature (black curve) at increasing total pressure for the Pd(100) at 1:1 ratio of CO and O_2. The red curve shows the corresponding oxygen coverage detected directly after light-off.

The intensity of the photoelectron peak, detected when gas is present in the chamber, is expressed by an additional factor to the relation of the peak intensity acquired in vacuum:

$$I_P = e^{\left(\frac{-x}{\lambda_e}\right)} \cdot I_0$$

where I_p is the intensity of the signal at pressure P, I_0 is the signal in vacuum, x is the distance that the electrons travel through the gas (pink area in Figure 5:3) and λ_e is the mean-free-path of the electron. With an increasing gas pressure the inelastic scattering is strongly increased towards lower kinetic energies. The inelastically scattered electrons contribute to an increased background. The intensity or area of the peaks reflect the concentration of the species on the surface, but the attenuation of the photoelectrons makes coverage determination from the APXPS spectra more complicated than for spectra obtained in UHV. In Figure 5:4b) the oxygen coverage on Pd(100) can be estimated by studying the area ratio of Pd $3p$ and O $1s$ in the O $1s$ region, and comparing this ratio with spectra measured at known oxygen

coverage in UHV. The maximum operating pressure is correlated to the aperture diameter, D_o and it has been found that a good working distance is $\sim 2D_o$ to avoid a significant pressure drop at the sample surface[94, 95] To fulfill the operating condition of UHV for the analyzer, differentially-pumped stages are located between the entrance aperture and the analyzer. APXPS setups also utilize electrostatic lenses in the analyzer to focus the electrons onto the apertures between the pumping stages resulting in an increased number of electrons reaching the detector. The gas phase between the aperture and an active surface during CO oxidation was studied in Paper XV, and the results are discussed in more detail in section 5.4.

5.2 Planar Laser Induced Fluorescence

The gas–surface interaction is an important parameter when different surface structures are formed. It is therefore of high relevance to understand the gas phase surrounding the surface when *in situ* studies are performed. The gas phase may provide new important information that can lead to a better understanding of the chemical reaction and kinetics at the surface. It is known that when flat surfaces such as single crystals are studied, a boundary layer builds up in the active regime and only a fraction of the reactants interact with the surface[96]. Another important application, where a known gas distribution in the chamber can contribute to further improvement is in the design of new reactors. Recently reported[96, 97] diverging results may be due to different reactor designs rather than different chemical mechanisms, because of flow configuration and build-up of a product boundary layer above surfaces. The flow and reactor geometry is, therefore, a critical parameter that should be considered when *in situ* experiments are carried out and analyzed.

Mass Spectroscopy (MS) is the most common way of detecting the gas composition in the reactor but do not generally contain any spatial information. This can be achieved by using capillary MS where a probe is used to sample the gas [98]. A probe, however, may disturb the gas flow and therefore also influence the chemical process. Fourier Transform Infra-Red Spectroscopy (FTIR) is capable of characterizing the gas phase non-intrusively. The drawback is that this method is based on absorption along a path, making it impossible to resolve the gas phase in the third dimension. To overcome these problems, Laser-induced Fluorescence (LIF) has been used to probe the gas. LIF is a common non-intrusive laser diagnostic technique for gas phase studies in many research fields such as atmospheric sciences, combustion physics and medicine [99-101] but is not as well-known to the catalytic community or

to the surface science community. Temperature, velocity and the concentration of the probed gas can be determined[102] using LIF, and this information can be obtained with high temporal resolution (10Hz) in two dimensions (2D) if a laser sheet is used to probe the gas. The technique is then referred to as Planar LIF, PLIF. Previous studies probing OH [103, 104], NO [105] or formaldehyde [106] in different reactions have been reported. The number of light sources with wavelength regions in the vacuum ultra violet (VUV) and infrared (IR), to probe CO and CO_2 respectively, are limited[107]. We have exploited recent developments in laser and detector technology and in Paper VIII we demonstrate the possibilities of probing CO_2 gas in 2D above a catalyst. This is investigated further in Paper IX and XIV where the spatial resolution makes it possible to compare the catalytic activity in a side-by-side experiment. In Paper X both the CO and CO_2 distribution is visualized during CO oxidation over a single crystal. The detailed analysis of the CO distribution in the vicinity of the crystal improves the interpretation of the APXPS gas phase analysis shown in Paper XI. In Papers XV and XIII, the spatial resolution is used to study the flow and geometry of the reactor.

5.2.1 Principle of operation

In LIF the gas is probed with a laser tuned to a wavelength that perfectly matches an energy level transition of the species of interest. If the wavelength is chosen wisely, the absorption cross section for the transition is high, and no other interfering molecules will have an overlapping transition at that specific energy. When the molecules relax, fluorescence light is emitted and can be detected. The pulse length of the laser determines the time interval the gas is irradiated and excited. If a laser sheet is used, gas molecules are excited within the irradiated volume, and a camera can then detect the fluorescence in 2D.

The detected signal is dependent on several physical parameters that have to be taken into account when the data is analyzed. Below, the expression for the LIF signal S_{LIF} in the linear excitation regime is shown,

$$S_{LIF} = \eta_c E g f(T) \sigma_0 \chi_{abs} \frac{P}{k_B T} \phi$$

where η_c is the experimental collection efficiency, E is the laser energy, g is a function that describes the spectral overlap between the laser and the absorption spectral lineshape, $f(T)$ is the Boltzmann fraction, σ_0 is the absorption cross section of the

detected species, χ_{abs} is the mole fraction of the detected species that together with P/k_BT gives the number density of the same species and ϕ is the fluorescence quantum yield. The fluorescence quantum yield represents the excited-state emission rates and the collisional interaction and energy transfer between the probed molecule and the carrier gas. The expression shows that the detected LIF signal is linearly dependent on the gas density and the fraction of molecules in the state from which the laser excites the molecule, *f(T)*. Collisional quenching occurs when the molecules relax non-radiatively through collisions, resulting in a signal loss which may be a problem if the number of gas molecules is high.

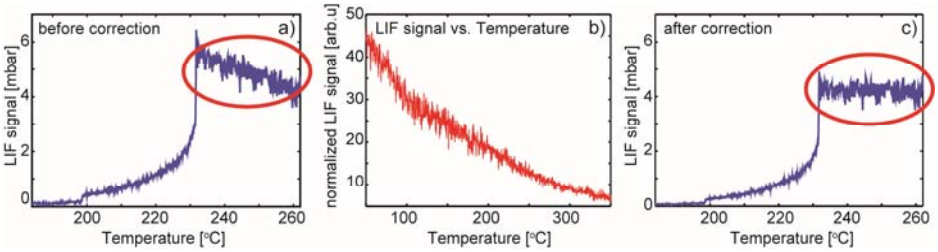

Figure 5:5 a) The plots show the raw LIF signal above the sample during CO oxidation when the temperature is ramped. The signal decreases linearly with the temperature, which is clear in the region marked with a red ellipse. b) The plot shows the raw LIF signal as a function of temperature. c) The raw data in a) compensated for the decreasing number of gas molecules according to the gas law.

The inverse temperature dependence of the LIF signal is illustrated by the plotted signal in Figure 5:5a). In the region indicated by a red ellipse a constant LIF signal is expected but instead a decreasing trend of the signal as a function of temperature is observed. The effect is investigated in more detail and the number of molecules 0.5 mm above the catalyst surface, as the temperature is increased, is illustrated in Figure 5:5b). The decreasing signal with the temperature is significant and has to be compensated for when the LIF data is analyzed. The LIF signal, where the temperature dependence has been taken into account in the evaluation process of the data is shown in Figure 5:5c).

5.2.2 CO and CO_2

The CO_2 molecule is probed in the infrared (IR) spectral regime. A laser system operated at 10 Hz generates the IR-laser light by difference-frequency mixing the output from a dye laser (PRSC-D-18, Sirah) at 763 nm with the fundamental frequency from a Nd:YAG laser (PRO 290-10, Spectra Physics) at 1064 nm in a

$LiNbO_3$ crystal. The resulting 2.7 µm laser beam with a pulse length of 5 ns was used to excite the ro-vibrational transition $(00^00) \rightarrow (10^01)$ in the CO_2 gas molecule, which is the antisymmetric stretch mode, see in Figure 5:6a). This transition is preferable due to the approximately 45 times higher cross section for excitation as compared to the 2.0 µm line[108] but weaker than the fundamental transition at 4.26 µm making absorption in the ambient air less prominent. The fluorescence light at 4.26 µm with a lifetime of approximately 100 µs was detected by an IR camera (Santa Barbara Focal Plane, SBF LP134) with a gate width of 15 µs, which is the limiting parameter for the temporal resolution.

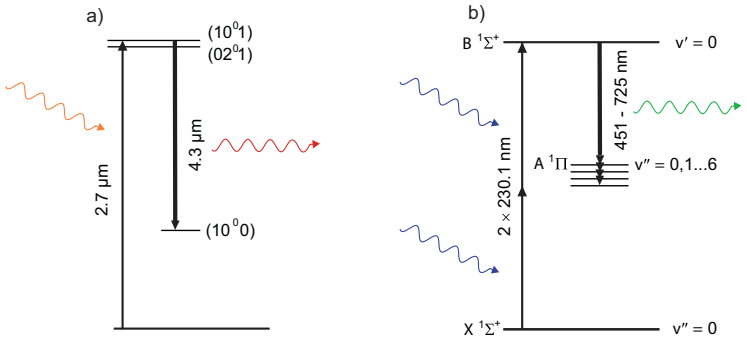

Figure 5:6 a) A schematic partial vibrational energy level diagram of CO_2. The $(00^00) \rightarrow (10^01)$ transition can be probed with a 2.7 µm wavelength of the laser [109]. The fluorescence is in the mid infrared region. b) In the case of CO, an electronic transition is probed via a two-photon process. The detected fluorescence light is in the visible spectral region.

The temperature of the environment in the setup plays an important role in the IR-PLIF measurement. The temperature of the probed gas will affect the population of the probed energy levels, and the thermal background is a general issue working in the infrared region. To discriminate the thermal background, the camera was triggered at 20 Hz, thus taking an extra image between every laser shot, making subtraction of the thermal background possible in the evaluation process of the data, see Figure 5:7.

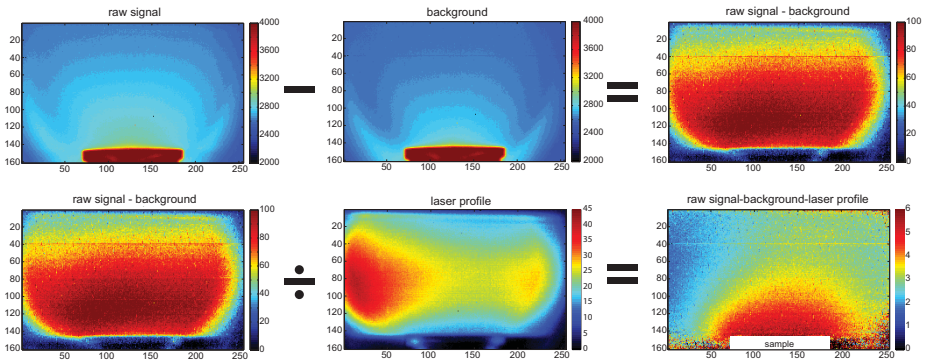

Figure 5:7 The strong IR signal from the thermal background (image without laser excitation of the gas) has to be subtracted from the raw data image in the analysis process, shown in the top panel. The temperature of the sample was around 250 °C when the images are taken. Further, the inhomogeneous laser sheet has to be taken into account if the CO_2 gas phase distribution should be visualized. In the lower panel the image of the laser profile is divided with the last image shown in the upper panel generating an image of the CO_2. A white rectangle is inserted to indicate where the sample is positioned.

CO is probed via an electronic transition in the VUV region. One difficulty working in the VUV region is the strong absorption in the ambient air, which induces a significant attenuation of the laser beam. To overcome this problem, a two-photon excitation with a wavelength of 230 nm can be used to reach the $B^1\Sigma^+ \leftarrow X^1\Sigma^+(0,0)$ transition in the so-called Hopfield–Birge band in the CO molecule. The third harmonic at 355 nm generated by a mode-locked Nd:YAG laser (PL2143C, Ekspla) with external amplifier (APL70-1100, Ekspla) pumps an Optical Parametric Generator (PG 401-P80-SH, Ekspla) that can be tuned to 230 nm. Fluorescence in the visible region with a wavelength between 450–660 nm is emitted when the molecule relaxes, and the A state is populated as illustrated in Figure 5:6b). The repetition rate was 10 Hz, and the 80 ps pulse duration provides high peak power, highly beneficial for the two-photon excitation process. Images were acquired using an f = 50 mm objective (Nikkor f/1.2) and a 36 mm extension tube mounted on an ICCD camera (PI-MAX3, Princeton Instruments). A long-pass filter (GG395, Schott) was used to suppress scattering and fluorescence from surfaces in the reactor.

The LIF signal is species-specific, making concentration measurements possible. Calibration measurements to correlate the detected CO and CO_2 signal were carried out at known partial pressures and a total pressure of 150 mbar see Figure 5:8. A linear dependency was observed for CO, but for CO_2, the curve bends downwards at around 10 mbar CO_2, which is mostly due to re-adsorption of CO_2 fluorescence

light. Re-adsorption of CO fluorescence is very unlikely, due to the two-photon process that is used to probe CO.

A number of parameters affect the spatial resolution such as imaging optics, the number of pixels and the pixel size in the camera, but also by the focus of the laser sheet. In the case of CO_2, the 6 mm laser sheet, which is a typically height of the laser sheet during the experiments, spans 75 × 256 pixel (the full sensor being 256 × 256 pixel) of the CO_2 detector resulting in 80 µm per pixel. In the case of CO, the sensor had a larger resolution of 1024 ×1024 pixel. To be able to capture images at 10 Hz, 2 × 2 binning had to be used, and each pixel corresponds to 30 µm. In the depth dimension (normal to the image plane), the resolution is given by the thickness of the laser sheet, which is ~300-400 µm in both cases.

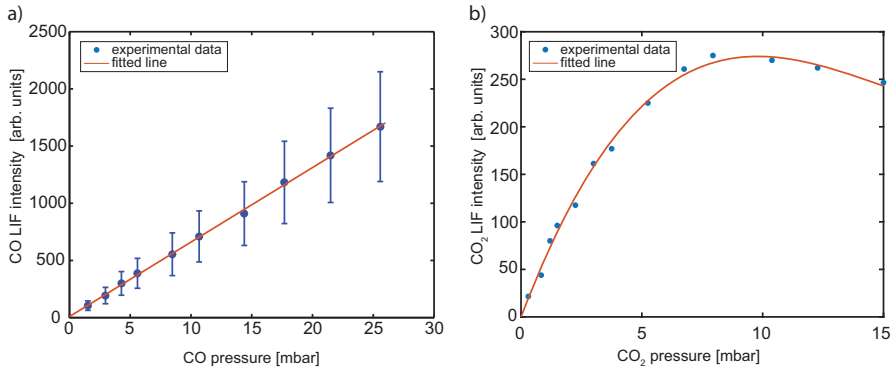

Figure 5:8 Calibration curve to convert the intensity of the PLIF signal to a partial pressure in mbar for CO in a) and CO_2 in b). The bent curve for CO_2 is mostly due to re-adsorption of the fluorescent light.

5.2.3 Experimental setups

The experimental setup is similar for probing/detecting CO and CO_2 and shown in Figure 5:9 a). In the following description of the setup, however, the CO_2 detection is used as an example. The laser beam is split up and ~10% of the light is guided to the reference cell with known CO_2 gas concentration, used for compensation of shot-to-shot fluctuations as well as wavelength jitter in the data evaluation process. The main laser beam is shaped into a laser sheet with a cylindrically shaped and spherical lens. The cylindrically shaped lens spread out the beam in one direction, and the spherical lens collimates the beam to a sheet and focuses it in the interrogation region. A pinhole is then used to adjust the height of the sheet, to around 0.1 mm above the surface of the sample, before it enters the reactor in a vertical fashion, see Figure 5:9a). The reactor is made of stainless steel and has five CaF_2 windows that

are transparent to the laser and fluorescence light in the mid-IR region. A camera, positioned perpendicular to the vertical laser sheet detects the fluorescence light from the probed gas molecule and a side view image of the gas distribution is recorded, Figure 5:9 b-c). By rotating the laser sheet, the gas can be probed parallel to the surface as shown in Figure 5:9 d-f). To detect the fluorescence light perpendicular to the laser sheet, a 45° tilted mirror is positioned at the top window to reflect the light into the camera and create a top view image of the gas phase. The reactor can easily be moved in x-, y- and z-direction with an accuracy of a micrometer. In figure 5:9 c) and f) the reactor is moved 1 mm in x- and z-direction respectively, in this case to visualize the CO_2 gas cloud over the active catalyst. This allows for a creation of a 3D model of the gas phase shown in Figure 5:9 g).

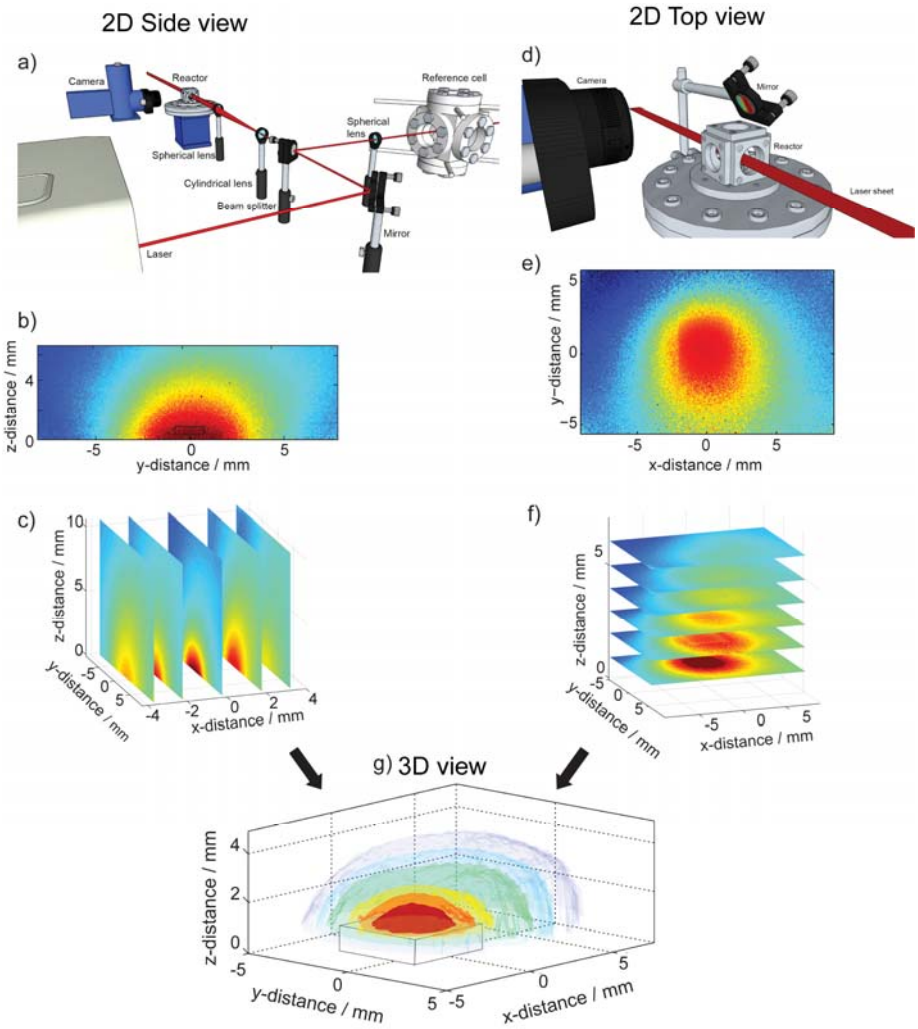

Figure 5:9 Schematic view of the experimental setup used to obtain an image of the gas phase in the vicinity of the active catalyst. a) The left panel shows a schematic view of the experimental setup when the vertical laser sheet probes the gas to obtain a side view image. b) An example of the side view image of the CO_2 gas above the catalyst. c) The laser sheet is systematically moved 1 mm for each image, and the gas can thereby be monitored over the surface. d) The right panel shows the modified setup, where a mirror is positioned to reflect in this case the CO_2 fluorescence through the top window, probed with a horizontal laser sheet. e) A top view image of the CO_2 gas phase. f) The corresponding measurement shown in c) but using top view cross section of the gas phase. The images in c) and f) is then used to create a 3D image of the gas phase, which is shown in g).

5.3 Gas visualization in the MTL regime

The spatial resolution of the gas phase obtained using PLIF makes it a powerful technique for *operando* studies of the gas phase in CO oxidation. A common problem when the activity of a catalyst is studied during CO oxidation, is that the reaction is mass transfer limited (MTL) by one of the reactants. It is therefore interesting to study the gas phase, in this highly active regime of the catalyst, in more detail.
The reaction is mass transfer limited when the diffusion of the products formed in the catalytic process, is slower than the catalytic reaction. The result is a lower partial pressure of the reactants close to the surface, which in turn affect the reaction rate. The reaction rate is no longer determined by the activity of the catalyst surface but rather reflects the flow conditions in the reactor. A build-up of a product boundary layer above the catalyst surface hinders the reactants to reach the active surface, and a 100% conversion of the limiting reactant is never observed. Instead, a lower plateau of a constant conversion that is independent of the temperature is observed. The exothermic CO oxidation reaction releases heat to the gas phase, which is not efficiently transported away. This lead to a temperature gradient within the boundary layer. The thickness of the boundary layer determines how efficient the heat can be transported away, but it also affects the mass transfer limitations where a thin boundary layer results in a more homogeneous gas distribution in the entire reactor. The PLIF image shown in Figure 5:9 b) was obtained in the MTL regime of a Pd(100) catalyst. The CO_2 boundary layer can be seen as a spherical cloud formed above the surface with a gradient of the CO_2 concentration out from the surface. In total, the CO_2 concentration within the boundary layer is higher as compared to the rest of the reactor. As a consequence, a depletion region of CO could be detected within the boundary layer, as reported in Paper X. A decrease of 80% of the initial CO partial pressure could be detected in the MTL regime in the vicinity of the surface, which can be compared to 30% of the initial CO partial pressure as detected by the MS, positioned at the outlet of the reactor.

5.4 Spatial resolution of the gas phase

The spatial resolution using PLIF makes it possible to follow the gas phase of a chemical reaction in 2D, and a detailed analysis of the distribution of the reactants and products during the process can be done. One of the advantages of using spatial resolution when performing experiments is the possibility to do comparison

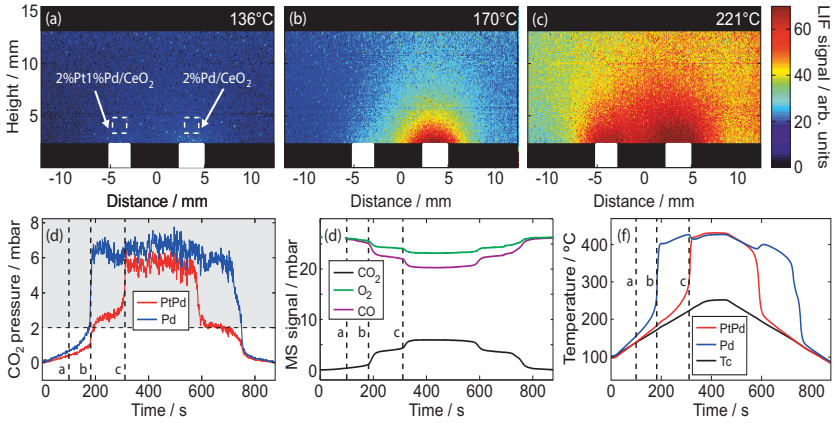

Figure 5:10 A comparison of two different powder catalysts supported by CeO_2 during CO oxidation. The gas conditions used was 18 ml_n/min CO, 18 ml_n/min O_2 and 36 ml_n/min Ar, at a total pressure of 150 mbar. a) The two inactive samples are positioned 8 mm apart in the reactor. b) At a temperature of 170°C the sample with pure Pd light-off, seen as an increased CO_2 production over the sample. c) At 221°C also the second sample light-off. d) The LIF signal extracted from an area (marked as a dashed rectangle in a)). e) The MS signal detected at the reactor outlet. f) The temperature recorded with an IR camera (red and blue) and with a thermocouple (black).

measurement under the same conditions and without repeating the experiment for different samples. This is clearly illustrated in Paper IX where we analyze the CO_2 gas phase in detail when CO oxidation is applied over two samples simultaneously in the reactor. In Figure 5:10 PLIF images acquired during CO oxidation over two powder samples are shown. The images show the CO_2 distribution over the samples, and it is found that the light-off temperature is lower for the catalyst with pure Pd as the active material as compared to the powder with a Pd and Pt mixture.

In Paper XIV a similar experiment as shown in Figure 5:10 is presented, but here we use a cylindrically shaped crystal (described in section 2.1.3). Instead of comparing two different catalytic materials, the effect of different step orientations is studied. The difference in light-off temperature at different positions of the crystal is found to be only 6 °C, which would be difficult to distinguish if it was not for the possibility to compare the step orientations simultaneously under the same conditions.

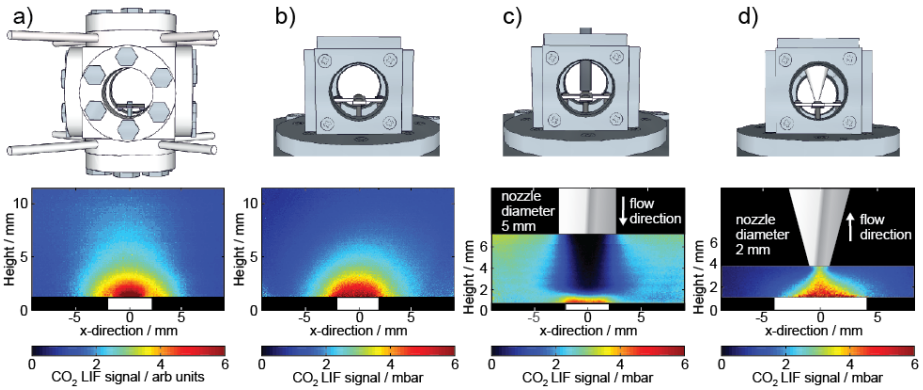

Figure 5:11 The gas distribution is characterized for four different reactors at a 1:1 ratio of CO and O_2. a) a 240 ml reactor flowing 45 mbar each of CO and O_2 in 90 mbar of Ar with a total pressure of 180 mbar (total flow of 72 ml_n/min), b) a 23 ml reactor flowing 6 mbar each of CO and O_2 in 138 mbar of Ar (total flow of 100 ml_n/min), c) a 23 ml reactor with a stagnation flow configuration flowing 6 mbar each of CO and O_2 in 138 mbar of Ar (total flow of 100 ml_n/min), d) a 23 ml reactor where the outlet is pumped through a 2 mm in diameter cone simulating an APXPS analyzer nozzle and flowing 6 mbar each of CO and O_2 in 138 mbar of Ar (total flow of 100 ml_n/min).

The spatial resolution has also been used to visualize how the geometry of the reactor affects the gas flow. In a theoretical study of the gas phase, Matera *et al.* report on a major difference in gas flow between various experimental *in situ* setups. Such differences make comparisons, of results conducted at different setups challenging[97]. Matera *et al.* simulate, by computational fluid dynamics, the complex gas flow pattern inside a reactor. The simulation illustrates how the cold gas entering the chamber creates a vortex rotating around the catalyst, eventually interacting with the surface, before reaching the outlet[110]. As a concequence of the complex flow pattern, the simulation indicates the importance of detecting the gas phase in the vicinity of the sample to be able to correlate surface structure with gas composition. The complex flow pattern also emphasizes that the geometry should be considered in the flow reactor design. This is studied in Paper XIII using our knowledge of a well-characterized CO_2 gas phase in the MTL regime where the gas phase is seen as a steady state. In Figure 5:11 four different reactors are shown together with a PLIF image of the CO_2 distribution in the MTL regime for each reactor. Reactors a) and b) have similar geometries and flow configurations but reactor a) is approximately 10 times larger in volume. The CO_2 gas distribution shown in the PLIF images, is almost identical for the two reactors even though a higher gas flow is utilized when the PLIF image is obtained in reactor b) compared to reactor a). In reactor c) a stagnation flow geometry has been considered where the gas inlet is via a tube from

the top, resulting in a gas flow in the direction towards the surface. The shape of the boundary layer is in good agreement with the simulation reported by Matera *et al.*[97], although they report on the O_2 as the minority reactant. The reactor in d), depicts a completely different shape of the boundary layer. This is a result of a flow configuration where the cone is used as an outlet, simulating the nozzle of a differential pumped APXPS electron analyzer. In Paper XIII we conclude that the CO_2 concentration close to the surface is similar in all reactors. The conditions determining when the formation of a boundary layer occurs, varies between the different reactors and flow configurations.

A more detailed investigation of how the flow and pressure affect the boundary layer in the highly active regime, when a reactor design shown in Figure 5:12Figure 5:11 d) is used, is presented in Paper XIII. The reactor setup is interesting because of the similarities of an APXPS setup. In an APXPS the nozzle of the analyzer is positioned approximately $2D$ (D=diameter of the analyzer aperture/nozzle) from the sample surface, as discussed in section 5.1.3. This is also the situation in reactor d) where the aperture is 2 mm in diameter and positioned 4 mm from the surface. The results are summarized in Figure 5:12 where the pressures and gas flow are varied generating different gas exchange rates (shown in the upper right corner in the images). The gas exchange rate expresses how often the gas is exchanged in the reactor. The operating pressure in APXPS is usually around one mbar and to keep the analyzer in UHV; it is heavily pumped. This makes the nozzle to the main outlet of the reactor and strongly affects the boundary layer. The study shows that the boundary layer is less defined when the flow rate is decreased, which is true also for higher pressures (see Figure 5:12d). The low flow rate generates a more batch like reactor where the whole reactor is filled with CO_2 a short while after the light-off. The results demonstrate that changing the pressure is not enough to mimic the gas phase at operating conditions of an industrial catalyst but also the flow needs to be considered to bridge the pressure gap. This can be concluded by comparing Figure 5:12g) and h) for 50 mbar in total pressure and Figure 5:12i) and j) for 20-25 mbar in total pressure.

We can only speculate on what the gas phase looks like for an operating industrial catalyst. In the case when CO oxidation is considered, we can assume that a boundary layer is formed similarly around a catalytically active nanoparticle as in Figure 5:12a), due to the high pressures and high flows in an industrial reactor. A similar gas phase distribution could probably also be generated at lower pressures but with a high flow rate, resulting in a boundary layer shown in Figure 5:12 g).

The lack of an oxide formation at a total pressure of 1 mbar, in the APXPS study in Paper VI and VII, indicates that the partial pressure of O_2 is too low in the vicinity of the surface in the MTL regime in these experiments to initiate oxidation. The conclusion is therefore that the total pressure in the reactor should be high enough that the resulting partial pressure of O_2 is sufficient to form an oxide on the surface in the MTL regime if the intention is to mimc the conditions for an operating industrial catalyst.

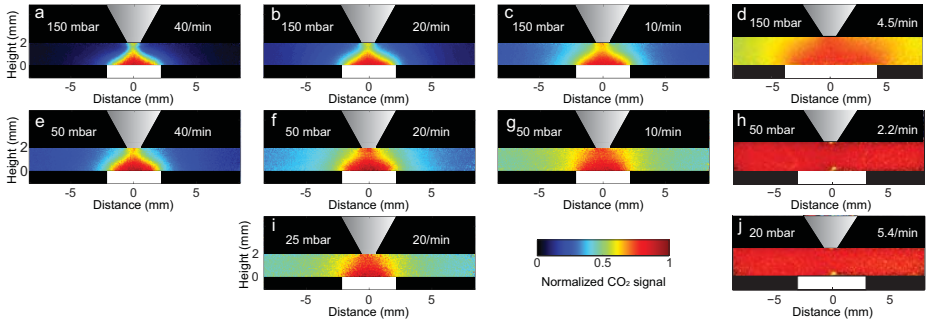

Figure 5:12 The CO_2 gas phase distribution between the surface and nozzle of the analyzer in a reactor that mimics the APXPS. The CO and O_2 ratio is 1 in all images, but the flow and partial pressures are varying with the total pressure. The gas exchange rate, determined by the gas flow is indicated in the upper right corner for each image. a-d) Total pressure of 150 mbar with a decreasing gas exchange rate in the chamber. The boundary layer is still detectable in d) but displaying less sharp gradients compared to a). e-h) Total pressure of 50 mbar with a decreasing gas exchange rate resulting in an increased CO_2 signal detected in the entire probed area. i-j) Total pressure of 25 and 20 mbar respectively where a boundary layer is detected in i) but not in j).

5.5 Surface characterization methods

Scanning Tunneling Microscopy (STM) and Low Energy Electron Diffraction (LEED) are two well-established surface science methods. Experimental stations at synchrotrons are often equipped with LEED for quality check of the samples after preparation. For theoretical support, density functional theory (DFT) is often used. In this thesis, STM and LEED results have been used for surface characterization of the model catalysts, prior to the use of *in situ* methods. The main techniques I have used are APXPS and PLIF, and STM, LEED and DFT is therefore only briefly discussed in the following sections.

5.5.1 Scanning Tunneling Microscopy

Scanning Tunneling Microscopy (STM) is a microscopy technique providing a real space image of the investigated surface capable of atomic resolution. The technique was invented at the IBM Zurich Laboratory by Binning and Rohrer[111], who were awarded the Nobel Prize in 1986. The technique is based on the quantum mechanical phenomenon called the tunneling effect and generates images of the atoms on the surface. In an STM, an atomically sharp tip should be used to generate a current of tunneling electrons between the conductive tip and surface when a bias is applied. The net current of electrons, I, that occurs is exponentially dependent on the tip- sample separation, d, (see Figure 5:13a) and is proportional to the number of states in the Fermi level of the sample[112].

$$I \propto e^{-\alpha d}$$

where α is a constant. The exponential dependency between the current and the tip-surface separation is utilized in the operation of the STM. A common operation mode is to keep the tunneling current constant by adjusting the tip-sample separation. The height adjustments represent the density of states of the surface and the tip, and a topographical image of the surface can be obtained by sweeping the tip within a few Ångströms above the surface as illustrated in Figure 5:13b). A more detailed description of the method can be found e.g. in[113, 114].

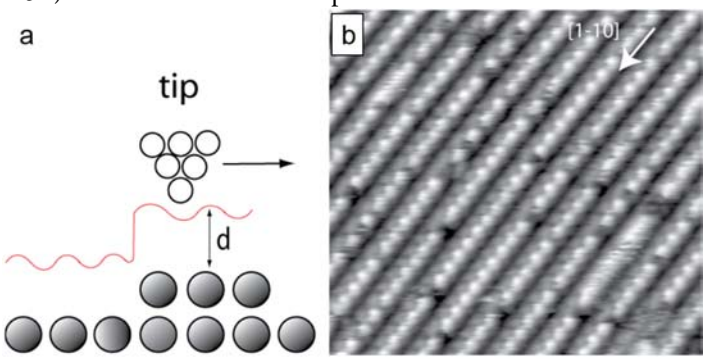

Figure 5:13 a) A schematic image of the STM operation. b) An STM image of a Pd(112) surface exposed to $1 \cdot 10^{-8}$ mbar of O_2 at 350 °C, with atomic resolution.

5.5.2 Low Energy Electron Diffraction

Low Energy Electron Diffraction (LEED) is used to study the periodicity and ordering of the surface. In 1927 Davisson and Germer performed the first LEED experiment, which was also the first confirmation of the wave property of electrons[115]. This makes it possible to study the diffraction pattern that arises when electrons are scattered at the surface. Electrons with a kinetic energy in the range of 100 eV, has a wavelength in the range of 1 Å, which is suitable for diffraction in a lattice with a periodicity on the order of atomic dimensions. Low energy electrons (10 – 1000 eV) have a short mean free path (below ~10 Å) and the diffraction pattern will therefore corresponds to the topmost atomic layers at the surface.

Experimentally, electrons from an electron gun impinge on the crystal surface, see Figure 5:14a). The potential difference between the filament generating the electrons and the sample defines the kinetic energy of the electrons and is variable. The electrons are backscattered and interfere constructively or destructively and the maxima are detected on a fluorescent screen. The detected LEED pattern represent the reciprocal lattice of the surface, which has the same shape as the real 2D lattice but rotated 90°, as illustrated in Figure 5:14b-c). LEED is a powerful tool to check the periodicity and the degree of ordering of single crystal surfaces. A more detailed description of the method can be found [116, 117]

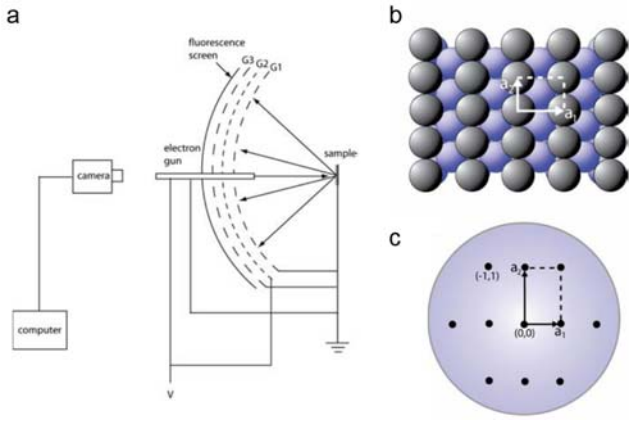

Figure 5:14 a) A schematic illustration of the LEED experimental setup. b) A model of a (110) surface. c) a schematic image of the LEED pattern from a (110) surface shown as a model in b).

5.5.3 Density Functional Theory

Theoretical calculations are a powerful tool to explore surface structures and support experimental findings, and Density Functional Theory (DFT) is widely used in the surface science community. DFT provides information about the energy of the system and specific parameters relevant for experimental results can be achieved. The theoretical contributions in this work are performed by collaborators, and have been used to support our experimental results. Only a brief introduction to the DFT is given here, but a complete description can be found e.g. in ref. [118, 119]. The theory is based on using the density of electrons to calculate the energies of a system by solving the Schrödinger equation. Finding the ground-state energy for a many-electron system, such as solids and large molecules is impossible due to a large number of parameters involved when the electron-electron interaction is taken into account. In the 60's, Hohenberg and Kohn [120] followed by Kohn and Sham[121] published a solution to this problem where they demonstrate that the many-electrons system can be treated as a one-electron problem (non-interacting system) by the use of a functional describing the electron density. The possibility to calculate the density of electrons for a solid makes it also possible to find a solution to this functional, which provides the ground state energy for the system. In the 90's, Perdew *et al.* [122] reported on an improved functional referred to as the PBE, which is extensively used today. This functional includes a gradient corrected exchange-correlation that compensates for a non-homogenous electron gas density in a solid.

6 Conclusions and Outlook

Part of the present thesis work has been devoted to oxidation studies of metals, alloys and nanoparticles relevant for catalysis. The motivation for such studies is that the oxygen induced structures may shed light on the active phase for a catalytic oxidation reaction. To this end, the oxidation of Pd, Rh and $Pd_{75}Ag_{25}$ single crystals with the (100) surface orientation as well as the corresponding nanoparticles, has been studied in detail. The oxidation experiments were performed *in situ* at pressures between 0.1 mbar and 1 mbar. At these pressures, a surface oxide is formed at approximately 150°C on Pd and Rh, and a thick bulk oxide is observed at higher temperatures. Our studies in Paper III and V show that a surface oxide with similar structure as on the Pd(100) also is formed on the $Pd_{75}Ag_{25}$(100) but at higher temperature. A bulk oxide on the $Pd_{75}Ag_{25}$ alloy is never observed (neither on the single crystal nor on the nanoparticles). We conclude that the nanoparticles (Pd, Rh, and $Pd_{75}Ag_{25}$) in the size of 10-35 nm follow a similar oxidation process as the single crystals but at slightly lower temperatures, which is partly explained by the high density of steps and kinks that result in a large number of undercoordinated atoms on the surface, facilitating oxygen dissociation.

We can also conclude that the oxides formed under the conditions discussed above, can be reduced by CO. The reduction process was followed *in situ* at pressures of 0.1 mbar as well as 5×10^{-8} mbar of CO and is suggested to proceed mainly via the borders of the reduced areas of the oxides of all investigated metals (Pd, Rh and PdAg alloy). The reduction process is much slower on the PdAg compared to the pure Pd, the slower process is probably related to the Ag layer at the interface between the $Pd_{75}Ag_{25}$ alloy and the oxide, which inhibits CO adsorption.

A large part of this thesis has been devoted to perform *in situ* studies of model catalyst surfaces during the catalytic oxidation of CO. The gas-surface interaction was studied by the use of APXPS and PLIF. The latter is a technique applied to catalysis developed in a collaboration between the divisions of Combustion Physics and Synchrotron Radiation Research and provides 2D images with high temporal resolution of the gas phase in the vicinity to the active catalytic surface.

The results from the oxidation studies discussed above was used in Paper VI and VII where an *in situ* structural study using APXPS was performed during CO oxidation. The results show an increasing oxygen coverage on the surface together with an increasing light-off temperature as the total pressure is increased from 10^{-6} to 1 Torr. We conclude that both the metallic and oxidized Pd surface was active while only an active metallic Rh surface was observed.

Ambient pressures XPS setups are continuously developed, and already today the technique can operate at higher pressures than 1 Torr. It would, therefore, be of great interest to study the CO oxidation over the model systems discussed above, at even higher pressure in an attempt to bridge the pressure gap. Also, the new generation of synchrotrons, such as MAX IV, which generate an even higher photon flux could make it possible to study the systems at higher pressure but also to increase the temporal resolution of the spectra.

To achieve a more complete picture of the CO oxidation reaction, the gas phase close to the active surface has been studied in detail. A boundary layer is observed in the MTL regime for CO oxidation. Within this boundary layer, the gas compositions are significantly different as compared to the rest of the reactor and measured by the MS at the outlet of the reactor. The boundary layer is strongly affected by the geometry of the chamber but also by the total pressure and gas flow.

The potential for applying PLIF in catalysis related research is significant, and here I will provide a short description of possible investigations and new applications. For instance, more studies of how the gas distribution is affected by the reactor geometry as well as pressures and flows should be conducted. This information could contribute to an optimized design of experimental setups for model catalysts, which could improve the link between industrial catalysts and model systems. Further, a more detailed investigation into the possibilities of extracting activation energies from the PLIF data should be of great interest for the catalysis community. A unique possibility of detecting short-lived radicals formed in the gas phase of the reaction would be a possible aim for future PLIF measurements, measurements that are extremely difficult with other techniques.

Several other reactions than CO oxidation can be studied using PLIF. One example is the NOx reduction process, where PLIF can provide an opportunity to follow NOx[105], the reducing agent NH_3, or intermediate radical distributions through the exhaust gas system of a diesel engine. Visualizing NOx and NH_3 in the exhaust

system could give insights that can lead to an improvement of the efficiency of the after-treatment system as well as for the engine itself.

PLIF characterizes the gas phase in a reaction with high temporal and spatial resolution and it would be beneficial to combine it with a surface sensitive technique. Recent results show that we can perform *operando* studies of CO oxidation over a Pd(100) crystal, where the surface structure is determined using High Energy Surface X-ray Diffraction (HESXRD)[123] simultaneously as the gas phase is detected using PLIF . Instead of using HESXRD, X-Ray Transmission Surface Diffraction (TSD)[124] could be used, which is a recently developed technique that also provides detailed information about the crystal structure. The benefit would be a setup, where the alignment is less sensitive. Illustrations of the HESXRD and TSD techniques are shown in Figure 6:1.

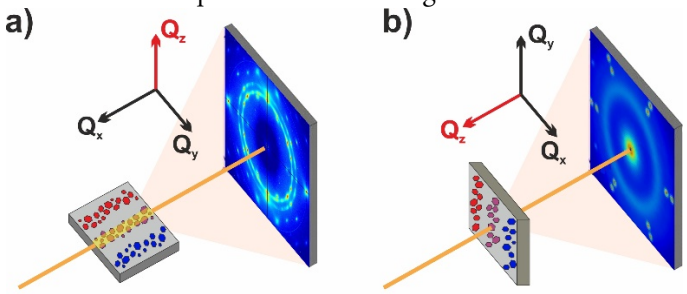

Figure 6:1 ***a)*** *HESXRD: a gracing incident beam leaves a large footprint on the sample and yields out-of-plane reciprocal space maps;* ***b)*** *TSD: the beam oriented normal to the sample. Illustration inspired by ref*[124]

The possibilities of detecting changes of the surface during catalytic reaction, in combination with PLIF, could also be done by studying the optical reflection from a LED light on the surface[125]. The relatively simple experimental setup used when studying the reflection from the surface as well as the high temporal resolution obtained, makes it a promising technique although it lacks the possibility to extract chemical information from the surface. To achieve detailed information about the chemical composition of the surface, Infrared Reflection-Absorption Spectroscopy (IRAS) is a powerful technique that also could be combined with PLIF.

One advantage using PLIF is that the gas phase can be spatially resolved making it possible to compare several catalysts under the same conditions in a side-by-side measurement. The experimental setup and the sample shape, appearance and characteristics could be explored to expand the number of catalysts that can be

studied simultaneously, which can lead to a more time efficient screening of catalysts in industry.

The high energy content of hydrocarbons makes them highly interesting for industry and the Fischer Tropsch process is widely used to produce hydrocarbon chains (for example fuel) from syngas. Previous studies have shown promising results of detecting for example dimethyl ether (DME), methane and methanol using PLIF or other laser diagnostic techniques[126], which opens up for investigations of the production of different liquid fuels and chemicals.

As a final remark it can be mentioned that laser diagnostic techniques, in general, have the advantage of being non-intrusive, not restricted by high pressure and can be achieved with high temporal and spatial resolution. This makes them an attractive tool for studying catalytic reactions under realistic conditions. The possibilities of using other laser-based techniques than PLIF as a compliment, could therefore be considered. Techniques such as Coherent Anti-stokes Raman Spectroscopy (CARS), Degenerate Four Wave Mixing (DFWM) and Raman spectroscopy can for instance be used to study the gas temperature in detail, investigate gases that does not fluoresce, or detect several gases simultaneously.

References

1. Chorkendorff I, Niemantsverdriet JW. *Concepts of modern catalysis and kinetics*, 2nd edn. Wiley-VCH: Weinheim, 2007.

2. Berzelius JJ. *Jber Chem* 1835, **15**.

3. Roberts MW. Birth of the catalytic concept (1800-1900). *Catal Lett* 2000, **67**, 1-4.

4. Ostwald W. *Annalen der Naturphilosophie* 1910, **9**.

5. Ertl G. Reactions at surfaces: from atoms to complexity. *Nobel Lecture* 2007.

6. Freund HJ, Meijer G, Scheffler M, Schlögl R, Wolf M. CO Oxidation as a Prototypical Reaction for Heterogeneous Processes. *Angew Chem Int Edit* 2011, **50**, 10064-10094.

7. Westerström R, Wang JG, Ackermann MD, Gustafson J, Resta A, Mikkelsen A*, et al.* Structure and reactivity of a model catalyst alloy under realistic conditions. *J Phys-Condens Mat* 2008, **20**, 184018.

8. Ertl G, Rau P. Chemisorption and Catalytic Reactions of Oxygen and Carbon Monoxide on a Palladium(110) Surface. *Surf Sci* 1969, **15**, 443-465.

9. Ackermann MD, Pedersen TM, Hendriksen BLM, Robach O, Bobaru SC, Popa I*, et al.* Structure and reactivity of surface oxides on Pt(110) during catalytic CO oxidation. *Phys Rev Lett* 2005, **95**, 255505.

10. Hendriksen BLM, Ackermann MD, van Rijn R, Stoltz D, Popa I, Balmes O*, et al.* The role of steps in surface catalysis and reaction oscillations. *Nat Chem* 2010, **2**, 730-734.

11. Lang B, Joyner RW, Somorjai GA. Low-Energy Electron-Diffraction Studies of Chemisorbed Gases on Stepped Surfaces of Platinum. *Surf Sci* 1972, **30**, 454-474.

12. Zambelli T, Wintterlin J, Trost J, Ertl G. Identification of the ''active sites'' of a surface-catalyzed reaction. *Science* 1996, **273**, 1688-1690.

13. Dahl S, Logadottir A, Egeberg RC, Larsen JH, Chorkendorff I, Törnqvist E*, et al.* Role of steps in N_2 activation on Ru(0001). *Phys Rev Lett* 1999, **83**, 1814-1817.

14. Hammer B. Special sites at noble and late transition metal catalysts. *Top Catal* 2006, **37**, 3-16.

15. Hammer B, Nielsen OH, Nørskov JK. Structure sensitivity in adsorption: CO interaction with stepped and reconstructed Pt surfaces. *Catal Lett* 1997, **46**, 31-35.

16. Ertl G, Knözinger H, Weitkamp J. *Handbook of heterogeneous catalysis*, 2nd edn. Wiley-VCH: Weinheim Germany, 2008.

17. Lundgren E, Over H. In situ gas-surface interactions: approaching realistic conditions - Foreword. *J Phys-Condens Mat* 2008, **20**, 180302

18. Kittel C. *Introduction to solid state physics*, 3d ed edn. Wiley: New York,, 1968.

19. Ashcroft NW, Mermin ND. *Solid state physics*. Saunders College: Philadelphia, 1976.

20. Lundgren E, Gustafson J, Mikkelsen A, Andersen JN, Stierle A, Dosch H*, et al.* Kinetic hindrance during the initial oxidation of Pd(100) at ambient pressures. *Phys Rev Lett* 2004, **92**, 046101.

21. Köhler L, Kresse G, Schmid M, Lundgren E, Gustafson J, Mikkelsen A*, et al.* High-coverage oxygen structures on Rh(111): Adsorbate repulsion and site preference is not enough. *Phys Rev Lett* 2004, **93**, 266103.

22. Løvvik OM, Olsen RA. Density functional calculations on hydrogen in palladium-silver alloys. *J Alloy Compd* 2002, **330**, 332-337.

23. Tao F, Dag S, Wang LW, Liu Z, Butcher DR, Bluhm H*, et al.* Break-Up of Stepped Platinum Catalyst Surfaces by High CO Coverage. *Science* 2010, **327**, 850-853.

24. Somorjai GA, Joyner RW, Lang B. Reactivity of Low Index [(111) and (100)] and Stepped Platinum Single-Crystal Surfaces. *P Roy Soc Lond a Mat* 1972, **331**, 335-346.

25. Hoogers G, King DA. Adsorbate-Induced Step-Doubling Reconstruction of a Vicinal Metal-Surface - Oxygen on Rh (332). *Surf Sci* 1993, **286**, 306-316.

26. Westerström R, Gustafson J, Resta A, Mikkelsen A, Andersen JN, Lundgren E*, et al.* Oxidation of Pd(553): From ultrahigh vacuum to atmospheric pressure. *Phys Rev B* 2007, **76**, 155410.

27. Gustafson J, Resta A, Mikkelsen A, Westerström R, Andersen JN, Lundgren E*, et al.* Oxygen-induced step bunching and faceting of Rh(553): Experiment and ab initio calculations. *Phys Rev B* 2006, **74**, 035401.

28. Walter AL, Schiller F, Corso M, Merte LR, Bertram F, Lobo-Checa J*, et al.* X-ray photoemission analysis of clean and carbon monoxide-chemisorbed platinum(111) stepped surfaces using a curved crystal. *Nat Commun* 2015, **6**, 8903.

29. Badan C, Farber RG, Heyrich Y, Koper MTM, Killelea DR, Juurlink LBF. Step-Type Selective Oxidation of Platinum Surfaces. *J Phys Chem C* 2016, **120**, 22927-22935.

30. Messing ME, Dick KA, Wallenberg LR, Deppert K. Generation of size-selected gold nanoparticles by spark discharge - for growth of epitaxial nanowires. *Gold Bull* 2009, **42**, 20-26.

31. Stierle A, Nolte P, Jin-Phillipp NY, Kasper N, Schulli TU, Dosch H. Shape changes of supported Rh nanoparticles during oxidation and reduction cycles. *Science* 2008, **321**, 1654-1658.

32. Kasper N, Stierle A, Nolte P, Jin-Phillipp Y, Wagner T, de Oteyza DG*, et al. In situ* oxidation study of MgO(100) supported Pd nanoparticles. *Surf Sci* 2006, **600**, 2860-2867.

33. Mittendorfer F, Seriani N, Dubay O, Kresse G. Morphology of mesoscopic Rh and Pd nanoparticles under oxidizing conditions. *Phys Rev B* 2007, **76**, 233413.

34. Tao F, Grass ME, Zhang YW, Butcher DR, Renzas JR, Liu Z*, et al.* Reaction-driven restructuring of bimetallic nanoparticle systems. *Abstr Pap Am Chem S* 2009, **237**, 833-833.

35. Mcelhiney G, Papp H, Pritchard J. Adsorption of Xe and Co on Ag(111). *Surf Sci* 1976, **54**, 617-634.

36. Wouda PT, Schmid M, Nieuwenhuys BE, Varga P. STM study of the (111) and (100) surfaces of PdAg. *Surf Sci* 1998, **417**, 292-300.

37. Vitos L, Ropo M, Kokko K, Punkkinen MPJ, Kollar J, Johansson B. Exceptional surface stability in late transition metal alloys driven by lattice strain. *Phys Rev B* 2008, **77**, 121401(R).

38. Steiner P, Hüfner S. Impurity D-Bands and Core Level Binding-Energy Shifts in Dilute Cu, Ag, Au and Pd Alloys. *Solid State Commun* 1982, **41**, 619-622.

39. Chen MS, Cal Y, Yan Z, Gath KK, Axnanda S, Goodman DW. Highly active surfaces for CO oxidation on Rh, Pd, and Pt. *Surf Sci* 2007, **601**, 5326-5331.

40. Over H, Kim YD, Seitsonen AP, Wendt S, Lundgren E, Schmid M*, et al.* Atomic-scale structure and catalytic reactivity of the RuO_2(110) surface. *Science* 2000, **287**, 1474-1476.

41. van Rijn R, Balmes O, Resta A, Wermeille D, Westerström R, Gustafson J, *et al.* Surface structure and reactivity of Pd(100) during CO oxidation near ambient pressures. *Phys Chem Chem Phys* 2011, **13**, 13167-13171.

42. McClure SM, Goodman DW. New insights into catalytic CO oxidation on Pt-group metals at elevated pressures. *Chem Phys Lett* 2009, **469**, 1-13.

43. Andersen JN, Qvarford M, Nyholm R, Sorensen SL, Wigren C. Surface Core-Level Shifts as a Probe of the Local Overlayer Structure - CO on Pd(100). *Phys Rev Lett* 1991, **67**, 2822-2825.

44. Uvdal P, Karlsson PA, Nyberg C, Andersson S, Richardson NV. On the Structure of Dense CO Overlayers. *Surf Sci* 1988, **202**, 167-182.

45. Chen R, Chen Z, Ma B, Hao X, Kapur N, Hyun J, *et al.* CO adsorption on Pt (111) and Pd (111) surfaces: A first-principles based lattice gas Monte-Carlo study. *Comput Theor Chem* 2012, **987**, 77-83.

46. Surnev S, Sock M, Ramsey MG, Netzer FP, Wiklund M, Borg M, *et al.* CO adsorption on Pd(111): a high-resolution core level photoemission and electron energy loss spectroscopy study. *Surf Sci* 2000, **470**, 171-185.

47. Strisland F, Ramstad A, Ramsvik T, Borg A. CO adsorption on the Rh(100) surface studied by high resolution photoelectron spectroscopy. *Surf Sci* 1998, **415**, L1020-L1026.

48. Lundgren E, Gustafson J, Resta A, Weissenrieder J, Mikkelsen A, Andersen JN, *et al.* The surface oxide as a source of oxygen on Rh(111). *J Electron Spectrosc* 2005, **144**, 367-372.

49. Wang J, Yun Y, Altman EI. The plasma oxidation of Pd(100). *Surf Sci* 2007, **601**, 3497-3505.

50. Todorova M, Lundgren E, Blum V, Mikkelsen A, Gray S, Gustafson J, *et al.* The Pd(100)-(√5x√5)R27°-O surface oxide revisited. *Surf Sci* 2003, **541**, 101-112.

51. Orent TW, Bader SD. Leed and Els Study of the Initial Oxidation of Pd(100). *Surf Sci* 1982, **115**, 323-334.

52. Gustafson J. Oxidation of some late transition metal surfaces: Structural studies from UHV to atmospheric pressure. Doctoral thesis, Lund University, Lund, 2005.

53. Baraldi A, Cerda J, Martin-Gago JA, Comelli G, Lizzit S, Paolucci G*, et al.* Oxygen induced reconstruction of the Rh(100) surface: General tendency towards threefold oxygen adsorption site on Rh surfaces. *Phys Rev Lett* 1999, **82**, 4874-4877.

54. Gustafson J, Lundgren E, Mikkelsen A, Borg M, Klikovits J, Schmid M*, et al.* The Rh(100)-(3 x 1)-2O structure. *J Phys-Condens Mat* 2012, **24**, 225006.

55. Mittendorfer F, Franz T, Klikovits J, Schmid M, Merte LR, Zaman SS*, et al.* Oxygen-Stabilized Rh Adatoms: 0D Oxides on a Vicinal Surface. *J Phys Chem Lett* 2011, **2**, 2747-2751.

56. Todorova M. Oxidation of Palladium Surfaces. Doctoral thesis, Technical Univeristy Berlin, Berlin, 2004.

57. Kostelnik P, Seriani N, Kresse G, Mikkelsen A, Lundgren E, Blum V*, et al.* The Pd (100)-(√5x√5)R27°-O surface oxide: A LEED, DFT and STM study. *Surf Sci* 2007, **601**, 1574-1581.

58. Stierle A, Kasper N, Dosch H, Lundgren E, Gustafson J, Mikkelsen A*, et al.* Surface X-ray study of the structure and morphology of the oxidized Pd(001) surface. *J Chem Phys* 2005, **122**, 044706.

59. Shipilin M, Hejral U, Lundgren E, Merte LR, Zhang C, Stierle A*, et al.* Quantitative surface structure determination using *in situ* high-energy SXRD: Surface oxide formation on Pd(100) during catalytic CO oxidation. *Surf Sci* 2014, **630**, 229-235.

60. Shipilin M, Stierle A, Merte LR, Gustafson J, Hejral U, Martin NM*, et al.* The influence of incommensurability on the long-range periodicity of the Pd(100)-(√5x√5)R27°-PdO(101). *Surf Sci* 2017, **660**, 1-8.

61. Seriani N, Harl J, Mittendorfer F, Kresse G. A first-principles study of bulk oxide formation on Pd(100). *J Chem Phys* 2009, **131**, 054701.

62. Rogal J, Reuter K, Scheffler M. Thermodynamic stability of PdO surfaces. *Phys Rev B* 2004, **69**, 075421.

63. Gustafson J, Mikkelsen A, Borg M, Andersen JN, Lundgren E, Klein C*, et al.* Structure of a thin oxide film on Rh(100). *Phys Rev B* 2005, **71**, 115442.

64. Gustafson J, Mikkelsen A, Borg M, Lundgren E, Köhler L, Kresse G*, et al.* Self-limited growth of a thin oxide layer on Rh(111). *Phys Rev Lett* 2004, **92**, 126102.

65. Blomberg S, Lundgren E, Westerström R, Erdogan E, Martin NM, Mikkelsen A*, et al.* Structure of the Rh_2O_3(0001) surface. *Surf Sci* 2012, **606**, 1416-1421.

66. Khanra BC, Menon M. Adsorption-introduced MC simulation technique for segregation studies in Pd-Ag nanoparticles. *Physica B* 2000, **291**, 368-372.

67. Hammer B, Nørskov JK. Why Gold Is the Noblest of All the Metals. *Nature* 1995, **376**, 238-240.

68. Hammer B, Nørskov JK. Theoretical surface science and catalysis - Calculations and concepts. *Adv Catal* 2000, **45**, 71-129.

69. Mavrikakis M, Stoltze P, Nørskov JK. Making gold less noble. *Catal Lett* 2000, **64**, 101-106.

70. Mavrikakis M, Hammer B, Nørskov JK. Effect of strain on the reactivity of metal surfaces. *Phys Rev Lett* 1998, **81**, 2819-2822.

71. Valden M, Lai X, Goodman DW. Onset of catalytic activity of gold clusters on titania with the appearance of nonmetallic properties. *Science* 1998, **281**, 1647-1650.

72. Honkala K, Hellman A, Remediakis IN, Logadottir A, Carlsson A, Dahl S, *et al.* Ammonia synthesis from first-principles calculations. *Science* 2005, **307**, 555-558.

73. Somorjai GA, Li Y. *Introduction to surface chemistry and catalysis*, 2nd edn. Wiley: Hoboken, N.J., 2010.

74. Gao F, McClure SM, Cai Y, Gath KK, Wang Y, Chen MS, *et al.* CO oxidation trends on Pt-group metals from ultrahigh vacuum to near atmospheric pressures: A combined in situ PM-IRAS and reaction kinetics study. *Surf Sci* 2009, **603**, 65-70.

75. Engel T, Ertl G. Surface Residence Times and Reaction-Mechanism in Catalytic-Oxidation of CO on Pd(111). *Chem Phys Lett* 1978, **54**, 95-98.

76. Hendriksen BLM, Bobaru SC, Frenken JWM. Oscillatory CO oxidation on Pd(100) studied with in situ scanning tunneling microscopy. *Surf Sci* 2004, **552**, 229-242.

77. Onderwaater WG, Balmes O, Roobol SB, Van Spronsen M, Drnec J, Carla F, *et al.* Oxidation of CO on Pd(100): on the structural evolution of the PdO layer during the self sustained oscillation regime. *Catalysis, Structure & Reactivity* 2017, **3**, 89-94.

78. Toyoshima R, Yoshida M, Monya Y, Kousa Y, Suzuki K, Abe H, *et al.* In Situ Ambient Pressure XPS Study of CO Oxidation Reaction on Pd(111) Surfaces. *J Phys Chem C* 2012, **116**, 18691-18697.

79. Hirvi JT, Kinnunen TJJ, Suvanto M, Pakkanen TA, Nørskov JK. CO oxidation on PdO surfaces. *J Chem Phys* 2010, **133**, 084704.

80. Matera S, Reuter K. First-Principles Approach to Heat and Mass Transfer Effects in Model Catalyst Studies. *Catal Lett* 2009, **133**, 156-159.

81. Kan HH, Weaver JF. A PdO(101) thin film grown on Pd(111) in ultrahigh vacuum. *Surf Sci* 2008, **602**, L53-L57.

82. Gustafson J, Westerström R, Mikkelsen A, Torrelles X, Balmes O, Bovet N, *et al.* Sensitivity of catalysis to surface structure: The example of CO oxidation on Rh under realistic conditions. *Phys Rev B* 2008, **78**, 045423.

83. Gustafson J, Westerström R, Resta A, Mikkelsen A, Andersen JN, Balmes O, *et al.* Structure and catalytic reactivity of Rh oxides. *Catal Today* 2009, **145**, 227-235.

84. Einstein A. Generation and conversion of light with regard to a heuristic point of view. *Ann Phys-Berlin* 1905, **17**, 132-148.

85. Siegbahn K. *ESCA applied to free molecules*. North-Holland Publishing: Amsterdam ; London, 1969.

86. Beutler A, Lundgren E, Nyholm R, Andersen JN, Setlik BJ, Heskett D. Coverage- and temperature-dependent site occupancy of carbon monoxide on Rh(111) studied by high-resolution core-level photoemission. *Surf Sci* 1998, **396**, 117-136.

87. Doniach S, Šunjić M. Many-Electron Singularity in X-Ray Photoemission and X-Ray Line Spectra from Metals. *J Phys Part C Solid* 1970, **3**, 285-291.

88. Ruppender HJ, Grunze M, Kong CW, Wilmers M. *In situ* X-Ray Photoelectron-Spectroscopy of Surfaces at Pressures up to 1 Mbar. *Surf Interface Anal* 1990, **15**, 245-253.

89. Pantförder J, Pöllmann S, Zhu JF, Borgmann D, Denecke R, Steinrück HP. New setup for *in situ* x-ray photoelectron spectroscopy from ultrahigh vacuum to 1 mbar. *Rev Sci Instrum* 2005, **76**, 014102.

90. Trotochaud L, Head AR, Karslioglu O, Kyhl L, Bluhm H. Ambient pressure photoelectron spectroscopy: Practical considerations and experimental frontiers. *J Phys-Condens Mat* 2017, **29**, 053002.

91. Bluhm H, Hävecker M, Knop-Gericke A, Kleimenov E, Schlogl R, Teschner D, *et al.* Methanol oxidation on a copper catalyst investigated using *in situ* X-ray photoelectron spectroscopy. *J Phys Chem B* 2004, **108**, 14340-14347.

92. Bluhm H. Photoelectron spectroscopy of surfaces under humid conditions. *J Electron Spectrosc* 2010, **177**, 71-84.

93. Axnanda S, Scheele M, Crumlin E, Mao BH, Chang R, Rani S*, et al.* Direct Work Function Measurement by Gas Phase Photoelectron Spectroscopy and Its Application on PbS Nanoparticles. *Nano Lett* 2013, **13**, 6176-6182.

94. Ogletree DF, Bluhm H, Hebenstreit ED, Salmeron M. Photoelectron spectroscopy under ambient pressure and temperature conditions. *Nucl Instrum Meth A* 2009, **601**, 151-160.

95. Bluhm H, Hävecker M, Knop-Gericke A, Kiskinova M, Schlögl R, Salmeron M. *In situ* x-ray photoelectron spectroscopy studies of gas-solid interfaces at near-ambient conditions. *Mrs Bull* 2007, **32**, 1022-1030.

96. Matera S, Reuter K. Transport limitations and bistability for in situ CO oxidation at RuO_2(110): First-principles based multiscale modeling. *Phys Rev B* 2010, **82**, 085446.

97. Matera S, Reuter K. When atomic-scale resolution is not enough: Spatial effects on in situ model catalyst studies. *J Catal* 2012, **295**, 261-268.

98. Roos M, Kielbassa S, Schirling C, Haring T, Bansmann J, Behm RJ. Scanning mass spectrometer for quantitative reaction studies on catalytically active microstructures. *Rev Sci Instrum* 2007, **78**, 084104.

99. Liao W, Case AT, Mastromarino J, Tan D, Dibb JE. Observations of HONO by laser-induced fluorescence at the South Pole during ANTCI 2003. *Geophys Res Lett* 2006, **33**, L09810.

100. Svanberg S. Medical Diagnostics Using Laser-Induced Fluorescence. *Phys Scripta* 1987, **T19b**, 469-475.

101. Aldén M, Wallin S, Wendt W. Applications of 2-Photon Absorption for Detection of CO in Combustion Gases. *Appl Phys B-Photo* 1984, **33**, 205-212.

102. Eckbreth AC. *Laser diagnostics for combustion temperature and species*. Abacus, 1988.

103. Försth M, Eisert F, Gudmundson F, Persson J, Rosén A. Analysis of the kinetics for the H_2+1/2 O_2 <-> H_2O reaction on a hot Pt surface in the pressure range 0.10-10 Torr. *Catal Lett* 2000, **66**, 63-69.

104. Gudmundson F, Persson JL, Försth M, Behrendt F, Kasemo B, Rosén A. OH gas phase chemistry outside a Pt catalyst. *J Catal* 1998, **179**, 420-430.

105. Zellner A, Suntz R, Deutschmann O. Two-Dimensional Spatial Resolution of Concentration Profiles in Catalytic Reactors by Planar Laser-Induced Fluorescence: NO Reduction over Diesel Oxidation Catalysts. *Angew Chem Int Edit* 2015, **54**, 2653-2655.

106. Kang W, Fujita O, Ito K. Visualization of formaldehyde distribution above platinum plate catalyst by using LIF method. *J Energ Resour-Asme* 1996, **118**, 82-87.

107. Li ZS, Rupinski M, Zetterberg J, Alwahabi ZT, Aldén M. Mid-infrared polarization spectroscopy of polyatomic molecules: Detection of nascent CO_2 and H_2O in atmospheric pressure flames. *Chem Phys Lett* 2005, **407**, 243-248.

108. Alwahabi ZT, Zetterberg J, Li ZS, Aldén M. High resolution polarization spectroscopy and laser induced fluorescence of CO_2 around 2 μm. *Eur Phys J D* 2007, **42**, 41-47.

109. Li ZS, Zetterberg J, Malm P, Aldén M. Investigation of infrared LIF detection of CO_2 in applied combustion diagnostics. *European Combustion Meeting*. Brussels; 2005.

110. Matera S, Maestri M, Cuoci A, Reuter K. Predictive-Quality Surface Reaction Chemistry in Real Reactor Models: Integrating First-Principles Kinetic Monte Carlo Simulations into Computational Fluid Dynamics. *ACS Catal* 2014, **4**, 4081-4092.

111. Binning G, Rohrer H, Gerber C, Weibel E. Surface Studies by Scanning Tunneling Microscopy. *Phys Rev Lett* 1982, **49**, 57-61.

112. Tersoff J, Hamann DR. Theory and Application for the Scanning Tunneling Microscope. *Phys Rev Lett* 1983, **50**, 1998-2001.

113. Meyer E, Hug HJ, Bennewitz R. *Scanning probe microscopy : the lab on a tip*. Springer: Berlin ; New York, 2004.

114. Hawkes PW, Spence JCH. Science of microscopy. New York: Springer,; 2007.

115. Davisson C, Germer LH. The scattering of electrons by a single crystal of nickel. *Nature* 1927, **119**, 558-560.

116. Van Hove MA, Weinberg WH, Chan CM. *Low-energy electron diffraction : experiment, theory, and surface structure determination*. Springer Berlin Heidelberg, 1986.

117. Kittel C. *Introduction to solid state physics*, 8d ed edn. Wiley: New York,, 2005.

118. Barth Uv. Basic Density-Functional Theory—an Overview. *Phys Scr* 2004, **T109**, 9-39.

119. Groß A. *Theoretical surface science : a microscopic perspective*. Springer: Berlin ; New York, 2003.

120. Hohenberg P, Kohn W. Inhomogeneous Electron Gas. *Phys Rev B* 1964, **136**, B864-B871.

121. Kohn W, Sham LJ. Self-Consistent Equations Including Exchange and Correlation Effects. *Phys Rev* 1965, **140**, 1133-1138.

122. Perdew JP, Burke K, Ernzerhof M. Generalized gradient approximation made simple. *Phys Rev Lett* 1996, 77, 3865-3868.

123. Gustafson J, Shipilin M, Zhang C, Stierle A, Hejral U, Ruett U*, et al.* High-Energy Surface X-ray Diffraction for Fast Surface Structure Determination. *Science* 2014, **343**, 758-761.

124. Reikowski F, Wiegmann T, Stettner J, Drnec J, Honkimaki V, Maroun F, *et al.* Transmission Surface Diffraction for *Operando* Studies of Heterogeneous Interfaces. *J Phys Chem Lett* 2017, **8**, 1067-1071.

125. Onderwaater WG, Taranovskyy A, Bremmer GM, Baarle GCv, Frenken JWM, Groot IMN. From dull to shiny: A novel setup for reflectance difference analysis under catalytic conditions. *Rev Sci Instrum* 2017, **88**, 023704.

126. Andersson O, Neij H, Bood J, Axelsson B, Aldén M. Optical characterization of dimethyl ether (DME) for laser-based combustion diagnostics. *Combust Sci Technol* 1998, **137**, 299-322.

Summary of papers

Oxidation and reduction of transition metals

The CO oxidation reaction has been investigated by a step-by-step approach, where the oxidation and reduction of the surfaces have first been studied separately. The systematic *in situ* studies of the Pd, Rh and $Pd_{75}Ag_{25}$, in high pressures (up to 1 mbar) of CO and O_2, provide information about formation and chemical composition of the different surface structures that can be present during CO oxidation under realistic conditions.

I. Oxidation and reduction of Pd(100) and aerosol-deposited Pd nanoparticles

This paper reports on a combined APXPS and DFT study where the oxidation and reduction of the Pd metal can be followed *in situ*. The Pd(100) was exposed to 0.5 mbar O_2 while increasing the temperature of the samples. At 270°C, a PdO(101) bulk oxide was detected at the Pd(100). The bulk oxide was investigated in detail, and an XPS component was assigned to the surface of the PdO film. The PdO surface component was identified by exposing the PdO to 0.5 mbar CO. The CO adsorb on the undercoordinated Pd atoms at the PdO surface, which shifts the surface related peak towards higher binding energy. The Pd nanoparticles showed a similar oxidation behavior but were oxidized at lower temperature. In addition, a carbide was observed at the nanoparticles during the reduction process.

II. A high pressure x-ray photoelectron spectroscopy study of oxidation and reduction of Rh(100) and Rh nanoparticles

Herein we report on an oxidation and reduction study, similar as in paper I, but of Rh. The Rh(100) was exposed to 0.1 Torr O_2, and the surface structure was observed *in situ* using high pressure XPS. At a temperature of 400°C, a bulk oxide was observed that was investigated further. The deconvolution of the spectra reveal a surface, as well as a bulk component. The sample was exposed to 0.1 Torr CO to reduce the bulk oxide and at a temperature of 260°C the bulk oxide is totally reduced. The 21 nm nanoparticles reveal a similar oxidation and reduction behavior as the Rh(100) but the bulk oxide was observed already at 340°C and was reduced at 170°C.

III. Surface composition of clean and oxidized $Pd_{75}Ag_{25}$(100) from photoelectron spectroscopy and density functional theory calculations

The article presents an oxidation surface study of the alloy of Pd and Ag with the composition 3:1. The clean as well as oxidized (100) surface was studied in UHV using X-ray photoelectron spectroscopy. The spectra supported by DFT calculations reveal that the clean surface is Ag terminated. When the alloy is exposed to oxygen Pd segregates to the surface and forms a similar surface oxide as on Pd(100), which has a periodicity of $(\sqrt{5}\times\sqrt{5})R27°$. The interface between the oxide and alloy bulk was determined to consist of a complete Ag layer.

IV. Reduction behavior of oxidized Pd(100) and $Pd_{75}Ag_{25}$(100) surfaces using CO

In this paper, XPS was used to study and compare the reduction of the oxidized surfaces of Pd(100) and $Pd_{75}Ag_{25}$(100). The reduction was followed in time at specific temperatures at pressures of $5x10^{-8}$ mbar. The reduction is suggested to proceed through reduced islands. The process is observed to be slower for the alloy than pure Pd, which is explained by DFT calculations that suggest an increased diffusion barrier for CO on the alloy due to the Ag layer underneath the oxide.

V. Generation and oxidation of aerosol deposited PdAg nanoparticles

This article considers a characterization and oxidation study of 10 and 17 nm $Pd_{75}Ag_{25}$ alloy nanoparticles. The nanoparticles were determined to consist of a 3:1 ratio of Pd and Ag and the large shift in the X-ray photoelectron spectra, as well as the transmission electron microscopy image, indicate that the particles are well mixed. The oxidation of the PdAg particles in 0.1 Torr O_2 was followed *in situ* using ambient pressure X-ray photoelectron spectroscopy and compared to the oxidation of $Pd_{75}Ag_{25}$(100) under the same conditions. Segregation of Pd to the surface leads to an oxide formation with a $(\sqrt{5}\times\sqrt{5})R27°$ periodicity, as previous reported in Paper III.

Structural studies of a catalyst during CO oxidation

The light-off temperature of the CO oxidation as a function of total pressure and oxygen coverage, has been studied for the (100) low index surfaces of Pd and Rh. Similar results are detected on both system where an increased light-off temperature in conjunction with increased oxygen coverage is detected as the total pressure is increased.

VI. *In situ* X-ray photoelectron spectroscopy of model catalysts: At the edge of the gap

Herein we have used APXPS for an *in situ* study of the Pd(100) surface structure during CO oxidation. The ratio of CO and O_2 was kept at 1:1 but the total pressure was increased. The results show that both the light-off temperature and the oxygen coverage after light-off increases with the total pressure. In a 1:1 ratio of CO and O_2 a metallic Pd surface was detected immediately after the light-off but if the ratio was changed to a more oxygen-rich conditions of 1:4 in a total pressure of 1 Torr, a surface oxide was observed. This is also supported by DFT calculations.

VII. A high pressure X-ray photoelectron spectroscopy study of CO oxidation over Rh(100)

In this study, we have used APXPS to *in situ* detect the surface structure of Rh(100) during CO oxidation in a total pressure ranging from 0.01 to 1 mbar. Similar results as reported on Pd(100) in Paper VI was observed. The results show an increasing oxygen coverage as well as increasing light-off temperature with the increasing total pressure where the ratio of CO and O_2 was 1:1. Also the ratio of 1:4 at a total pressure of 0.66 mbar was conducted. For the conditions used in this study, the oxidized surface was never observed, but an active Rh metal could be detected.

Gas phase visualization in the vicinity of a catalyst surface

The gas-surface interaction is essential for the surface structure and crucial when the active phase of the catalyst should be determined. The gas phase has therefore been studied using Planar Laser-Induced Fluorescence, which is a well-known technique in combustion studies but less in the field of catalysis. The technique is species specific and provides a spatial resolution of the gas distribution with high temporal resolution. The results presented in this thesis are based on pressures between 25 and 150 mbar.

VIII. An *in situ* set up for the detection of CO_2 from catalytic CO oxidation by using planar laser-induced fluorescence

This paper shows the first results from CO_2 detection over a Rh(553) crystal during CO oxidation using planar laser-induced fluorescence. The article describes the experimental setup and clearly illustrates the potential of using PLIF in catalysis research for spatial information of the gas phase.

IX. Spatially and temporally resolved gas distributions around heterogeneous catalysts using infrared planar laser-induced fluorescence

In this article, we demonstrate the potential of extracting important gas phase information by using PLIF. The result shows how the CO_2 is distributed over the catalyst surface during CO oxidation. A boundary layer is formed around the sample with completely different gas composition as compared to the rest of the reactor. The paper reports on simultaneous measurement of parallel catalysts during CO oxidation where the light-off temperature of the different catalysts was determined.

X. Real-time gas phase imaging over a Pd(110) catalyst during CO oxidation by means of planar laser-induced fluorescence

Herein we report on spatially resolved gas phase detection of CO and CO_2 over a Pd single crystal using planar laser-induced fluorescence. The boundary layer formed around the active catalyst surface in the highly active regime is visualized both in CO_2 and CO PLIF measurements. The CO_2 and CO images are in good agreement where a strong signal of CO_2 overlap with an absent of CO signal. The CO partial pressure in the mass transfer limit regime is investigated in more detail and an inhomogeneous CO pressure is observed over the sample surface. The results also show a decrease of approximately 80% of the signal, 0.3 mm over the sample surface, which can be compared to a decrease of 20-30% detected by the mass spectrometer at the outlet of the reactor.

XI. Comparison of AP-XPS and PLIF measurements during CO oxidation over Pd single crystals

This study investigates the gas phase close to the catalyst surface during CO oxidation in an AP-XPS set up. The CO gas phase photoemission peaks are correlated with the detection of CO using PLIF. The lack of CO gas phase signal in the AP-XPS spectra in the highly active regime is most probably because the concentration is below the detection limit for the AP-XPS setup.

XII. Evidence for the active phase of heterogeneous catalysts through *in situ* reaction product imaging and multiscale modeling

This is mainly a theoretically work where DFT calculations are combined with fluid dynamical simulations and used to interpret the LIF trace of CO_2 over a Pd(100) single crystal during CO oxidation. By comparing theoretical results with the experimentally detected data, the active phase of the catalyst is suggested to be metallic.

XIII. 2D and 3D imaging of the gas phase close to an operating model catalyst by planar laser induced fluorescence

This is a topical review paper where the experimental setup as well as several examples are shown of detecting CO_2, CO, and NH_3. The results highlight the information PLIF provides by detecting the gas phase with spatial resolution. The measurements can be done both from a side view and a top view making it possible to create a 3D image of the gas phase in the mass transfer limit regime. The gas distribution in the reactor is demonstrated to be dependent on the reactor geometry and gas flows, by using PLIF. The temporal resolution of 10 Hz also allows for following self-sustained oscillations of the catalytic reaction.

XIV. Strain dependent light-off temperature in catalysis revealed by planar laser-induced fluorescence

The study shows the advantage of the spatial resolution provided by PLIF, by comparing the light-off temperature for two different step orientations. The cylindrically shaped crystal used in the experiment exposes two different step orientations that can be compared under the same conditions by the use of PLIF. A 6°C lower light-off temperature was detected for the B-type step as compared to the A-type step, which is supported by DFT calculations.

XV. Visualization of gas distribution in a model AP-XPS reactor by PLIF: CO oxidation over a Pd(100) catalyst

The article discusses the gas distribution between the sample and aperture of the nozzle to the detector in an AP-XPS setup. The images show a distorted boundary layer caused by the nozzle that is used as a gas outlet in the setup. The study also covers a pressure (25 - 150 mbar) and gas flow dependent measurement where the boundary layer of CO_2 is present under most of the investigated conditions.

XVI. Combining synchrotron light with laser technology in catalysis research

The paper describes the first *operando* experiments where PLIF is combined with High Energy Surface X-ray Diffraction (HESXRD). CO oxidation over Pd(100) was studied and the surface structure could be correlated with the production of CO_2. The results highlight the importance of detecting the gas phase in the vicinity of the catalyst surface and thereby enable the correlation between the active surface structure and the gas phase environment.